Journal of Quantitative Spectroscopy & Radiative Transfer 130 (2013) 201–219

Contents lists available at ScienceDirect

Journal of Quantitative Spectroscopy & Radiative Transfer

journal homepage: www.elsevier.com/locate/jqsrt

Methane line parameters in the HITRAN2012 database

L.R. Brown [a,*], K. Sung [a], D.C. Benner [b], V.M. Devi [b], V. Boudon [c], T. Gabard [c], C. Wenger [c], A. Campargue [d], O. Leshchishina [d], S. Kassi [d], D. Mondelain [d], L. Wang [d], L. Daumont [e], L. Régalia [e], M. Rey [e], X. Thomas [e], Vl. G. Tyuterev [e], O.M. Lyulin [f], A.V. Nikitin [f], H.M. Niederer [g], S. Albert [g], S. Bauerecker [g], M. Quack [g], J.J. O'Brien [h], I.E. Gordon [i], L.S. Rothman [i], H. Sasada [j], A. Coustenis [k], M.A.H. Smith [l], T. Carrington Jr. [m], X.-G. Wang [m], A.W. Mantz [n], P.T. Spickler [o]

[a] Jet Propulsion Laboratory, California Institute of Technology, 4800 Oak Grove Dr., Pasadena, CA 91109, USA
[b] Department of Physics, The College of William and Mary, Box 8795, Williamsburg, VA 23187, USA
[c] Laboratoire Interdisciplinaire Carnot de Bourgogne, UMR 6303 CNRS–Université de Bourgogne 9 Av. A. Savary, BP 47870 F-21078, Dijon Cedex, France
[d] Université Grenoble 1/CNRS, UMR5588 LIPhy, Grenoble F-38041, France
[e] Groupe de Spectrométrie Moléculaire et Atmosphérique, UMR CNRS 7331, Université de Reims, 4. U.F.R. Sciences, B.P. 1039, 51687 Reims Cedex 2, France
[f] Laboratory of Theoretical Spectroscopy, V.E. Zuev Institute of Atmospheric Optics, SB RAS, Academician Zuev square, 634021 Tomsk, Russia
[g] Laboratorium für Physikalische Chemie, ETH Zürich, CH-8093 Zürich, Switzerland
[h] Department of Chemistry and Biochemistry, University of Missouri, St. Louis, MO 63121-4400, USA
[i] Harvard-Smithsonian Center for Astrophysics, Atomic and Molecular Physics Division, Cambridge, MA 02138, USA
[j] Department of Physics, Faculty of Science and Technology, Keio University, 3-14-1, Hiyoshi, Kohoku-ku, Yokohama 223-8522, Japan
[k] Laboratoire d'Etudes Spatiales et d'Instrumentation en Astrophysique (LESIA), Observatoire de Paris, CNRS, UPMC Univ. Paris 06, Univ. Paris-Diderot, 5, place Jules Janssen, 92195 Meudon Cedex, France
[l] Science Directorate, NASA Langley Research Center, Hampton, VA 23681, USA
[m] Chemistry Department, Queen's University, Kingston, Ontario, Canada K7L 3N6
[n] Department of Physics, Astronomy and Geophysics, Connecticut College, 270 Mohegan Avenue, New London, CT 06320, USA
[o] Department of Physics, Bridgewater College, Bridgewater, VA 22812, USA

ARTICLE INFO

Article history:
Received 4 April 2013
Received in revised form
13 June 2013
Accepted 19 June 2013
Available online 28 June 2013

Keywords:
Methane
Line parameters
Remote sensing
Planets
Exoplanets
HITRAN database

ABSTRACT

The compilation of methane molecular line parameters was updated to include new global analyses and measurements for $^{12}CH_4$, $^{13}CH_4$ and $^{12}CH_3D$. Over 70% of the methane parameters in HITRAN2008 were replaced; existing parameters retained were the microwave lines and the Dyad of $^{13}CH_4$ near 7 μm and ν_6 of $^{13}CH_3D$ near 8.7 μm, $^{12}CH_3D$ (7–4076 cm^{-1}), hot bands of $^{12}CH_4$ (1887–3370 cm^{-1}) and normal sample CH_4 (4800–5550 cm^{-1} and 8000–9200 cm^{-1}). With a minimum intensity at 296 K in units of cm^{-1}/(molecule cm^{-2}) set to 10^{-37} for the far-IR and 10^{-29} for the mid- and near-IR, the methane database increased from 290,091 lines in HITRAN2008 to 468,013 lines, and three-fourths of these involved the main isotopologue. For $^{12}CH_4$ and $^{13}CH_4$, bands from the ground state were revised up to 4800 cm^{-1}. For the first time, $^{13}CH_4$ and $^{12}CH_3D$ line parameters near 2.3 μm were included. Above 5550 cm^{-1}, the new compilation was based on empirical measurements. Prior laboratory results were replaced with extensive new measurements using FTIR (5550–5852 cm^{-1}), differential absorption spectroscopy (DAS) and Cavity Ring Down Spectroscopy (CRDS) (5852–7912 cm^{-1}). Ground state *J* values for nearly half of the measured lines in this range were obtained, either by confirming quantum assignments of analyses or by using spectra at 80 and 296 K. Finally, over 11,000

* Corresponding author. Tel.: +1 818 354 2960, +1 626 260 4298.
E-mail address: linda.r.brown@jpl.nasa.gov (L.R. Brown).

0022-4073/$ - see front matter
http://dx.doi.org/10.1016/j.jqsrt.2013.06.020

measured positions, intensities and empirical lower state energies (obtained using cold CH_4) were also added for the first time between 10,923 and 11,502 cm^{-1}. Available pressure broadening measurements from HITRAN2008 were transferred into the new compilation, but 99% of the lines were given crudely-estimated coefficients. New measured intensities and broadening coefficients were included for far-IR transitions, and high accuracy line positions were inserted for the stronger P, Q and R branch transitions of ν_3 at 3.3 μm and $2\nu_3$ at 1.66 μm.

1. Introduction

Complete and accurate spectroscopy of methane is required for remote sensing of gaseous atmospheres. The various methane-containing targets in the universe involve a wide range of atmospheric temperatures, from less than 50 K for outer planets and their moons to more than 3000 K for exoplanets; thus the temperature dependence of spectroscopic features is crucial. Different astronomical atmospheres are mixtures of methane with other dominant species (air, N_2, H_2, He, etc.) so that reliable pressure-broadened line-shape information is very important. Table 1 lists an overview of what would be needed to provide the ideal methane compilation for universal remote sensing. Traditionally, the HITRAN database was focused on the needs of the Earth observations and only recently were the more extensive spectroscopic requirements of the outer planets considered. The newest HITRAN edition for methane greatly expands the information required for the cold and cooler planets (< 350 K) in terms of the completeness of the database, but future research is needed to support evolving exoplanet studies [1]. In addition, the Earth atmospheric applications now request better accuracy (sub-1%) [2] for the intensities and broadening parameters of stronger transitions in important regions; this will in turn require extensive future studies with non-Voigt line profiles (line mixing, speed dependence, collisional narrowing).

Remote sensing requires compilations that are sufficiently complete and accurate to meet the needs of specific applications. The far- and mid-IR methane spectra are better characterized by theoretical models for the transitions arising from the ground state and nine hot bands (whose transitions lie between 9 and 10 μm), but at shorter wavelengths, theoretical analyses become difficult because the number of interacting states increases very rapidly. This is seen in Fig. 1 where the vibrational states of methane are plotted in different colors. Quantum mechanical studies can provide the parameters to compute methane features in planetary spectra (purple) up to ~6200 cm^{-1}; however, for Earth studies, the predictions above 4800 cm^{-1} are not yet sufficiently accurate. Above 6200 cm^{-1} astronomers often resort to low resolution absorption cross sections (red) at shorter wavelengths [3].

To have a complete database for these applications, it is essential that very detailed and complete theoretical models be implemented to predict line positions, intensities, lower state energies and broadening coefficients within the desired accuracies. Extensive measurements are needed to produce and validate such calculations because the fitted constants of effective polyad Hamiltonians and dipole transition moments must be obtained by modeling the experimental data. Line-by-line assignment and fits of experimental spectra are tedious and difficult tasks that can only progress slowly by considering one polyad after the other, in increasing order of energy. Significant progress has been realized recently for $^{12}CH_4$ [4–6], and in a more limited manner for $^{13}CH_4$ [7,8]. As discussed later, useful initial values of the model parameters can be estimated by the *ab initio* and effective Hamiltonian approaches to facilitate interpretation of the higher polyads; such an approach with a subsequent empirical optimization permitted new assignments in $^{13}CH_4$ spectra [7]. In turn, new fitted parameters could

Table 1
Overview of database requirements for remote sensing of methane.

	Earth ***Very accurate***	**Outer planets** ***←In between→***	**Exoplanets etc.** ***Very complete***
Wavelength range (μm)	1.3–9	0.6–500	0.6–9
Temperature range (K)	180-350	40-200	300–3000
Minimum intensity[a]	10^{-26}	10^{-29}	??
Number of lines needed	~0.5 Million	10 Million	> 1 Billion
Pressure broadening species	N_2, O_2, H_2O	H_2, He, N_2	H_2, N_2?
Accuracies needed			
Positions (in cm^{-1}) [b]	0.0001	0.001–0.100	0.002–5
Intensities (%)	0.5–3	2–5	10–20
Line shapes (%)[c]	0.5–3 Non-Voigt	2–5 Non-Voigt	10–20 Voigt

[a] In cm^{-1}/(molecule cm^{-2}) at 296 K.
[b] In high pressure atmospheres, accurate pressure shifts are required as well.
[c] Line shapes: Lorentz, speed dependence, collisional narrowing and/or line mixing.

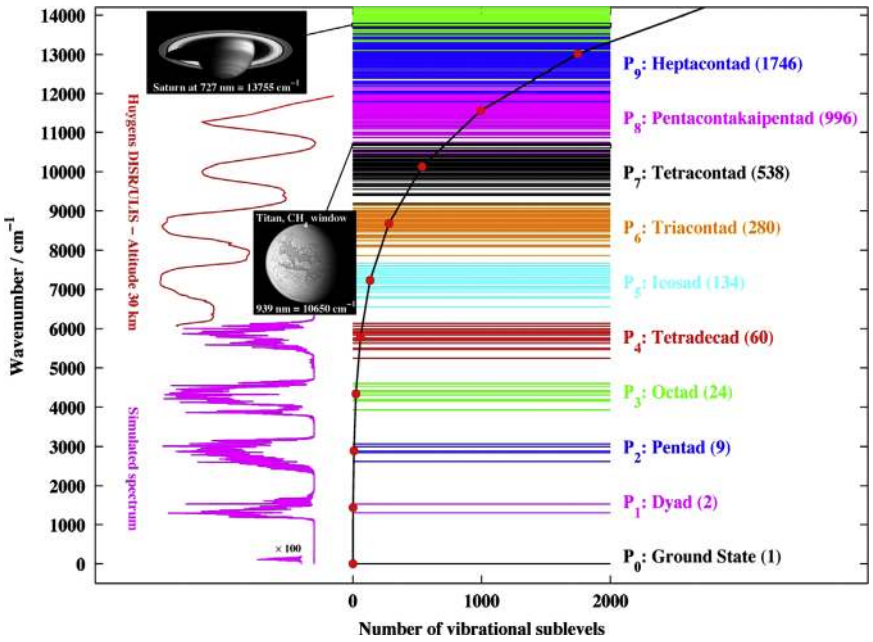

Fig. 1. The vibrational energy states of CH_4 which fall within distinct groups (Polyads=P_0, P_1, P_2 etc.). These are also designated by the number of unique vibrations: Dyad=2 (ν_2, ν_4), Pentad=5 ($2\nu_2$, ν_3, ν_1, $\nu_2+\nu_4$, $2\nu_4$), Octad=8 etc. Some of the vibrations have multiple *sub-vibrational* components; the total number for each polyad is shown in parentheses (and also plotted (red dots) as a function of the horizontal scale). The spectra at the left are: (*top*) a low resolution observation of Titan by the Huygens DISR/ULIS instrument onboard the Cassini spacecraft, (*bottom*) a computed methane spectrum based on line parameters predicted by theoretical models [5]. (To understand the use of color in this figure, please see the web version of this paper.)

Table 2
Status of theoretical modeling of measurements (state-of-the-art) for $^{12}CH_4$. The maximum J fitted, the number of measured positions and intensities and root mean square deviation (in cm^{-1} and % respectively) analyzed in each spectral region are shown for each polyad. The "Line profiles" column concerns purely calculated broadening coefficients for the indicated perturbers. The status of measurements is described later.

Polyad–spectral region	Line positions[a]	Line intensities[b]	Line profiles
0 – *Ground state* 0–200 cm^{-1} (> 50.0 μm)	Complete to J≤20 P_0–P_0 40 lines, 54 kHz P_1–P_1 20 lines, 200 kHz P_2–P_2 16 lines, 40 kHz	Complete to J≤18 P_0–P_0 92 lines, 9% P_1–P_1 96 lines, 9%	N_2
1 – *Dyad* 1000–1800 cm^{-1} (5.6–10.0 μm)	Complete to J≤23 P_1–P_0 1353 lines, 0.14 mk P_2–P_1 1023 lines, 0.55 mk	Complete to J≤22 P_1–P_0 1189 lines, 3.4% P_2–P_1 882 lines, 5.2%	He, N_2
2 – *Pentad* 2200–3300 cm^{-1} (3.0–4.6 μm)	Complete to J≤22 P_2–P_0 4412 lines, 0.61 mk P_3–P_1 1699 lines, 3.34 mk	Complete to J≤17 P_2–P_0 2586 lines, 3.0%	He, Ar, H_2, N_2, O_2, CH_4
3 – *Octad* 3700–4800 cm^{-1} (2.0–2.7 μm)	Good to J≤21 P_3–P_0 10626 lines, 3.53 mk	Partial analysis J≤14 P_3–P_0 3411 lines, 10.4%	N_2
4 – *Tetradecad* 4800–6300 cm^{-1} (1.6–1.9 μm)	Partial to J≤15 P_4–P_0 3012 lines, 23.1 mk	Initial analysis J≤14 (45 Sub-bands) P_4–P_0 1387 lines, 13.9%	None
5 – *Icosad* 6350–7700 cm^{-1} (1.3–1.5 μm)	Initial analysis J≤15 (Three band systems of 20) P_5–P_0 1995 lines, 3 mk	Initial analysis J≤15, P_5–P_0 1447 lines, 13.2%	None
Upper polyads **> 7800 cm^{-1}** (< 1.28 μm)	None	None	None
Windows between polyads (far wings, all regions)	Partial	Partial	None

[a] 1 mk = 0.001 cm^{-1} for line positions.
[b] % is 100 × (obs–calc)/calc for line intensities.

then be applied to improve the potential energy and dipole moment surfaces. The state of current modeling is summarized by polyad in Tables 2 and 3.

In the new HITRAN methane compilation, the positions and intensities up to 4800 cm^{-1} are based mostly on these model calculations [4,5,7,8]. While the newest Tetradecad

Table 3
Status of theoretical modeling of measurements (state-of-the-art) for $^{13}CH_4$. The number of measured values (data) and root mean square deviation are given for the transitions analyzed in each spectral region. The "Line profiles" column concerns purely calculated broadening coefficients for the indicated perturbers.

Polyad #–spectral region	Line positions[a]	Line intensities[b]	Line profiles
0 – *Ground state* 0–200 cm^{-1} (> 50.0 μm)	Complete to $J \leq 19$ P_0–P_0 27 lines, 38 kHz P_1–P_1 9 lines, 36 kHz	None ($^{12}CH_4$ values used)	None
1 – *Dyad* 1000–1800 cm^{-1} (5.6–10.0 μm)	Complete to $J \leq 20$ P_1–P_0 839 lines, 0.063 mk	Complete to $J \leq 11$ P_1–P_0 200 lines, 3.8%	He, H_2
2 – *Pentad* 2200–3300 cm^{-1} (3.0–4.6 μm)	Complete to $J \leq 21$ P_2–P_0 3089 lines, 0.47 mk	Complete to $J \leq 15$ P_2–P_0 485 lines, 4.4%	None
3 – *Octad* 3700–4800 cm^{-1} (2.0–2.7 μm)	Preliminary: $J \leq 9$ P_3–P_0 1837 lines, 4.63 mk	None (Work in progress)	None
Polyads above 4800 cm^{-1} *Tetradecad, Icosad, etc.*	None	None	None

[a] mk = 0.001 cm^{-1} for line positions.
[b] % is 100 × (obs–calc)/calc for line intensities.

Table 4
The HITRAN database for methane from 1982 to present.

HITRAN Year (Ref.)	# of Lines	[a]Min IR intensity	Max (cm^{-1})	[b]# of Species	Revision in positions and intensities	Revised (cm^{-1})
2012 [9]	**468,013**	**1×10^{-29}**	**11,502**	**4**	**72% of Lines replaced and new bands added**	**0–11,502**
2008 [10]	290,091	1×10^{-29}	9200	4	Change predictions New $^{12}CH_3D$ New $^{13}CH_3D$	0–3300 3200–3700 959–1694
2004 [11]	251,440	8×10^{-29}	9200	3	16% New	Above 4800
2001 [12][c]	211,465	8×10^{-29}	6185	3	82% Changed	600–5500
1996 [13]	48,035	1×10^{-24}	6185	3	Changed CH_3D (intensity)	900–1700
1992 [14]	47,415	4×10^{-28}	6107	3	$^{12}CH_4$ and $^{13}CH_4$ New/changed CH_3D New hot bands	0–6185 904–2356 2–1969
1986 [15]	17,774	4×10^{-24}	6107	3	Changed New CH_3D New: four hot bands	2255–3255 1100–1500 1530–3156
1982 [16]	11,803	3×10^{-24}	4667	3	CH_3D	7–100

[a] In units of cm^{-1}/(molecule cm^{-2}) at 296 K. The minimum values include the minor isotopologues whose infrared intensities are normalized to natural abundances; the minimum does not include far-IR transitions whose intensities are as low as 10^{-37} cm^{-1}/(molecule cm^{-2}) at 296 K.
[b] The four species are $^{12}CH_4$, $^{13}CH_4$, $^{12}CH_3D$ and $^{13}CH_3D$ (the last one added in 2008).
[c] Summary is for 2001 "updated" database given on line, not the initial 2000 compilation.

(P_4) analysis [6] permits quantum assignments (and thus lower state energies) to be made for many observed features, the predicted positions and intensities are still not sufficiently accurate for terrestrial atmospheric remote sensing. For this reason, the remainder of the database above 4800 cm^{-1} is taken from numerous line-by-line measurements.

2. Overview of the 2012 update for methane

During the last 40 years, the breadth and depth of methane spectroscopic compilations have expanded greatly [9–17]. The first compilation [17] contained only a few thousand transitions between 8 and 3.2 μm (for five stronger bands of $^{12}CH_4$ and two bands of $^{13}CH_4$). By 1986, transitions up to 1.6 μm were included, and as seen in Table 4, the number of lines and wavelength coverage continually increased as better theoretical quantum-mechanical modeling of the methane vibrational states developed to understand new and extensive laboratory measurements. Table 4 also reveals that major improvements tended to evolve on a decadal time scale.

An overview of the contents is shown in Table 5 and in Fig. 2; in the graph, the line intensities are plotted on a log scale as a function of wavenumber (cm^{-1}).

In this update, large portions of the $^{12}CH_4$ and $^{13}CH_4$ lists from HITRAN2008 were replaced, and some new regions were included for the first time: $^{12}CH_4$ near 11,200 cm^{-1}; $^{13}CH_4$ and CH_3D from 4000 cm^{-1} to ~4600 cm^{-1} with $^{13}CH_4$ greatly extended above 5850 cm^{-1}. The only parameters retained from HITRAN2008 are summarized in Table 6 by species giving the spectral region, the date of the last

Table 5
Summary of the new compilation for methane.

Species	# Bands	# Lines	Minimum (cm^{-1})	Maximum (cm^{-1})	Min intensity[a]	Max intensity[a]	Sum intensity[a]
$^{12}CH_4$	229	336,830	0.00106	11,501.8725	1.00×10^{-37}	2.114×10^{-19}	1.764×10^{-17}
$^{13}CH_4$	54	72,420	0.03177	11,318.5369	4.10×10^{-34}	2.363×10^{-21}	1.858×10^{-19}
$^{12}CH_3D$	48	54,550	7.76018	6510.3242	3.53×10^{-30}	5.714×10^{-23}	8.812×10^{-21}
$^{13}CH_3D$	3	4213	959.39399	1694.1234	2.77×10^{-29}	1.398×10^{-25}	3.150×10^{-23}
Total	**334**	**468,013**	**0.00106**	**11501.8725**	$\mathbf{1.00 \times 10^{-37}}$	$\mathbf{2.114 \times 10^{-19}}$	$\mathbf{1.783 \times 10^{-17}}$

[a] In units of cm^{-1}/(molecule cm^{-2}) at 296 K. The minimum values include the minor isotopologues whose infrared intensities are normalized to natural abundances.

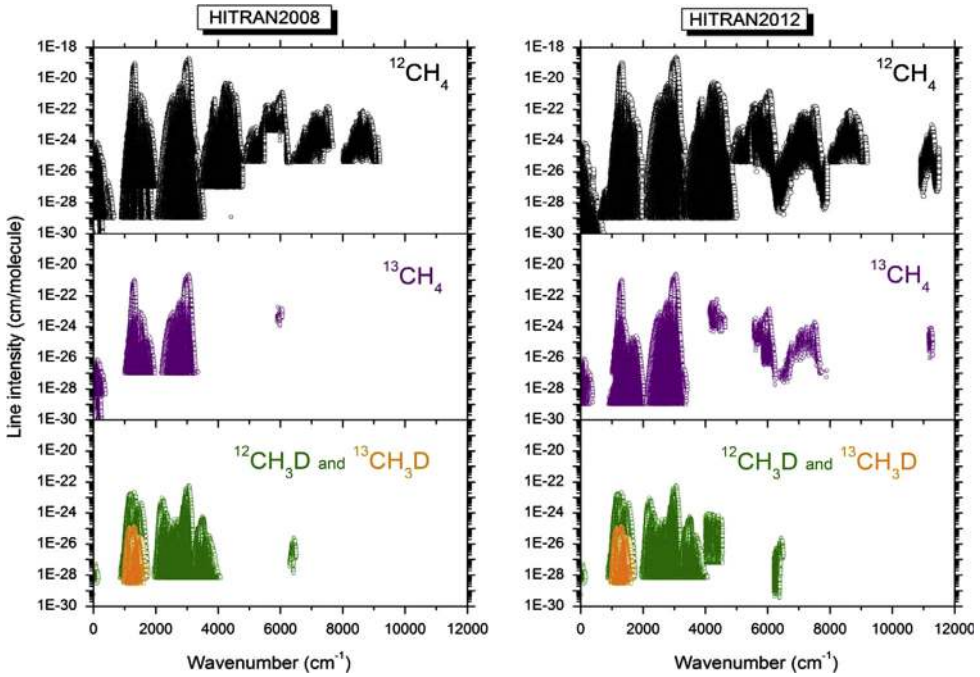

Fig. 2. Methane lines in HITRAN2008 (left panel) and HITRAN2012 (right panel) as a function of cm^{-1} for the four isotopologues. The intensities are in units of cm^{-1}/(molecule cm^{-2}) at 296 K. The numbers of individual lines for each isotopologue are given in Table 5.

Table 6
Lines retained from HITRAN2008 [10].

Species	Region in cm^{-1}	Last updated	# Lines
$^{12}CH_4$	1887–3370[a]	2008	9384
$^{12}CH_4$	4800–5550	2004	5017
$^{12}CH_4$	8002–9199	2004	17,882
$^{13}CH_4$	0.03–2.69	2001	119
	998–1571		2895
$^{12}CH_3D$	7–4076	2004	44,773
$^{13}CH_3D$	959–1694	2008	4213

[a] Hot bands only.

change and the number of lines. Further details about the new methane list are given in Section 3 for parameters between 0 and 4800 cm^{-1}; in Section 4 for the 4800–11,502 cm^{-1} range and in Section 5 for pressure broadening coefficients.

3. Sources of new line parameters from 0 to 4800 cm^{-1}

An overview of the new parameters in this range from recent research is given for three methane species in Table 7. The columns indicate the number of lines for individual regions along with the polyads of cold and hot bands included in each spectral interval and the sources of the data [4,5,7,8,10,18–21 and the references therein].

Except for CH_3D at 2.3 μm [21], the new database was based mainly on theoretical "global" modeling of the ground state, Dyad, Pentad and Octad polyads of $^{12}CH_4$ and $^{13}CH_4$. In this process, the best experimental positions and intensities in each region were selected and fitted simultaneously (see Tables 2 and 3). The work for the $^{12}CH_4$ parameters [4,5] modeled over 17,000 observed positions and over 8000 line intensities. The global analysis of the $^{13}CH_4$ involved more limited data in the Octad and Pentad [7,8]. To form the database, $^{12}CH_4$ and $^{13}CH_4$ transitions stronger than a chosen minimum value were included.

Table 7
New methane line parameters below 4800 cm^{-1} (mostly from model predictions).

Species	Region in cm^{-1}	Bands	Total # of lines	Refs.
$^{12}CH_4$	0–200	GS–GS	610	[4,18]
	0–740	Dyad–Dyad, Pentad–Pentad	66,985	[4,18]
	927–3454	Dyad–GS, Pentad–GS	46,538	[4,5,19]
	3322–5008	Octad–GS	87,798	[4,5]
	589–2303	Pentad–Dyad,	31,611	[4]
		Octad (mostly $3\nu_4$)–Pentad	2658	
	4633–4871	$2\nu_3-\nu_4$ (Experimental)	165	[20]
$^{13}CH_4$	14–3427	GS–GS, Pentad–GS	30,028	[7,8]
	90–2004	Dyad–Dyad, Pentad–Dyad	37,338	[8]
	4135–4642	Octad–GS	783	[8]
$^{12}CH_3D$	4000–4554	11 Bands (partial empirical list)	4085	[21]

Table 8
Example of recomputed positions of $^{12}CH_4$ using empirical upper states E'.

Position (obs)	Assignment[a]							Lower state E''	Upper state E'	Ave obs E' and rms	Obs–ave E'
	J'	C'	α'	J''	C''	α''	Band				
4414.0900	7	E	43	6	E	1		219.9134	4634.0034		0.0005
4340.8336	7	E	43	7	E	1	$\nu_3+\nu_4$ $1F_1$	293.1700	4634.0036	4634.0028	0.0008
4257.2651	7	E	43	8	E	1		376.7355	4634.0006	(0.0011)	−0.0023
4257.1822	7	E	43	8	E	2		376.8211	4634.0034		0.0008
3035.8086	7	E	43	7	E	2	$\nu_3+\nu_4-\nu_4$	1598.1948	4634.0035	Not used	0.0006

[a] Line positions, energies and rms are in cm^{-1}; in the database, the vibrational ID of $\nu_3+\nu_4$ $1F_1$ is written as 0 0 1 1 1F1 and the ground state is 0 0 0 0 1A1; α is an index within the polyad scheme indicating the nth energy level having the rotational symmetry E.

For some transitions, the measured positions were clearly more accurate than the predicted values and so many were recomputed using the known assignments to form empirical upper state levels. An example is shown in Table 8 using one specific energy level of $\nu_3+\nu_4$ of $^{12}CH_4$. Four transitions from the ground state were found along with one hot band line in the 3.3 μm region. To compute an empirical upper state, the calculated ground-state energy [4,5] was added to each measured line position to obtain an *experimental* upper-state energy seen in the table. In this case, the rms of this average was better than the observed–calculated model value (in this example, obs–calc = −0.0037 cm^{-1}) obtained from the global fits. In addition, if the group of known assignments contained one individual observed empirical upper state noticeably different from the rest (as in Table 8), the averaged upper state E' was then recomputed, omitting the largest deviating value. In the end, for this upper state level, all the positions of four Octad–GS transitions were recomputed for the new compilation using an *observed* empirical upper state based on three consistent transitions. While most hot band lines were not used directly, they provided evidence of consistent frequency calibrations for the three polyads (Dyad, Pentad and Octad). However, we note that line positions of the Octad–Dyad hot bands retained from HITRAN2008 were not changed using this procedure.

This process was applied for entries up to 4800 cm^{-1} for those vibration–rotation levels with two or more confirmed quantum assignments, i.e. for both cold and hot bands. For positions not changed, the accuracy code was set equal to "1" to mark those based on the unaltered prediction while the changed entries were given accuracy codes of 3 or 4. It should be noted that a very good rms of the averaged upper state energy represents a "precision" of the level and that the "absolute accuracy" also depends on the frequency calibration standards used by individual studies.

In addition to changes for line positions, a few other specific modifications were made based on empirical measurements. In HITRAN2008 [10], the calculated far-IR intensities for the ground state rotational transitions (GS–GS) were scaled by a factor of 1.15 based on new measurements of cold methane manifolds [22]. However, newer intensities [18] measured at the SOLEIL Synchrotron indicated that line-by-line intensities were closer to the original values in earlier versions of HITRAN [11] so this result was applied to the GS–GS intensities in the new 2012 compilation. One version of an *ab initio* calculation [23] confirmed the choice of a lower value, although there is no general agreement on this point (as discussed in Section 7.2). We note that only the GS–GS intensities were changed; they depend on the centrifugal distortion parameter which lies in the micro-Debye range. The Dyad–Dyad intensities were not scaled in 2008 because they depend on different parameters, in the milli-Debye range.

Note that the quality and the completeness of data for various bands are not homogeneous. As $^{12}CH_4$ does not

have a permanent dipole moment, the intensities of "forbidden" rotational GS–GS transitions are very difficult to measure accurately. This also concerns intensities of hot bands for which accurate intensity determinations are quite sparse. For this reason, intensity data for the corresponding bands could not yet be considered as firmly established. More measurements and calculations are still necessary to make reliable extrapolations for some of them.

The frequencies of stronger $^{12}CH_4$ transitions at 3.3 μm were newly measured with very high absolute accuracies (10^{-7}–10^{-6} cm^{-1}) using a 3.4 μm Difference Frequency Generation (DFG) spectrometer for sub-Doppler resolution saturated absorption spectroscopy [19,24]. For the database, these experimental positions replaced the values obtained from the global fits or the empirical upper states to expand the use of methane lines as frequency calibration standards. The changes involved only the specific measured transitions but not other transitions to the same upper state level. Available results for other isotopologues [25] and seven Q branch transitions of $^{12}CH_4$ [26] were not used, however.

For the first time, the database includes one $^{12}CH_4$ hot band, $2\nu_3$–ν_4 of the Tetradecad–Dyad [20] from Reims long-path spectra, three strong bands of the $^{13}CH_4$ Octad (ν_1+ν_4, ν_3+ν_4, ν_2+ν_3) from Zurich spectra [7], and several CH_3D bands between 4000 and 4550 cm^{-1} [21] from JPL and Kitt Peak FTS spectra.

In general, the Octad region of both $^{12}CH_4$ and $^{13}CH_4$ requires further measurements and analyses to reach the level of good accuracies achieved for the lower polyads. While the use of empirical upper states improved some line positions, there were still a number of insufficiently assigned vibrational states to predict reliable positions and intensities for all transitions up to J=15. In the interim, some measured $^{12}CH_4$ intensities [27] from HITRAN2008 were used in the new compilation. The new study of the $^{13}CH_4$ Octad [7] reported measured line positions and determined quantum assignments for some of the stronger bands. However, no intensities were retrieved, and the effective intensity model for the main isotopologue was applied for the $^{13}CH_4$ prediction. A comparison of calculated spectra with FTIR laboratory spectra of $^{13}CH_4$ revealed problems with many weaker lines; therefore only several hundred strong lines of three $^{13}CH_4$ bands were included this time. Given the accuracy requirements shown in Table 1, these faults may not be noticed by astronomers, but some atmospheric users with high resolution techniques do require a complete list with better accuracies. Some intensities of the weaker $^{12}CH_4$ Octad bands require improvements, and corresponding assignments must be confirmed as well. Interim updates will be made as new measurements and analyses become available.

For $^{12}CH_3D$, 4085 line positions and intensities were measured between 4000 and 4550 cm^{-1} using high resolution FTIR spectra recorded with enriched gas samples (98% D) at room and cold (80 K) temperatures [20]. To form a new linelist, the lower-state energies were identified for all the observed features; these were obtained by extending approximately 1000 reported quantum assignments [28] using effective Hamiltonian and dipole moment expansion models [29].

4. Sources of new line parameters from 4800 to 11,502 cm^{-1}

Above 4800 cm^{-1}, the theoretical modeling becomes very challenging, and much more effort is needed to provide reliable predictions, even for the Tetradecad and Icosad (see Fig. 1). Therefore, the bulk of the 2012 database for this region was taken from extensive line-by-line laboratory measurements reported by many different studies [30–59]. An overview of the new measurements from 5550 to 11,502 cm^{-1} is given in Table 9.

Quantum assignments were known for some measured lines so that the corresponding lower state energies could be included. For many other spectral features, empirical lower states were obtained from measured intensities at cold and room temperature data. Directly-measured broadening coefficients were attached for a relatively small number of transitions, but most broadening coefficients were rough estimates inserted as a function of lower-state J (either from the assignment or inferred from an empirical lower state); lines without the lower-state energies were given default constants for the pressure broadening parameters. This is detailed later in Section 5.

Table 9
New methane line parameters above 4800 cm^{-1} (from empirical measurements).

Species	Region in cm^{-1}	Total # of lines	Knowledge of Lower State J	Refs.
$^{12}CH_4$	5550–5855	5439	968 from assigned ν_2+ν_3+ν_4, ν_3+2ν_4	[31]
	5855–6205	9123	2464 from measured E_{emp}	[32]
			1049 lines of ν_1+ν_3, 2ν_2+2ν_4, 2ν_3, 2ν_2+ν_3, ν_1+2ν_2, 3ν_2+ν_4	[31]
			112 High accuracy 2ν_3 positions	[53]
	6205–7919	43,187	17603 measured E_{emp} with 2586 assigned to 5ν_4, ν_2+4ν_4 and ν_2+2ν_3	[32] [48,58,59]
	10,923–11502	11,242	Positions, intensities, E_{emp}	[65]
$^{13}CH_4$	5850–7899	4683	(2ν_3, ν_2+ν_3+ν_4 (only J''))	[32]
$^{12}CH_3D$	6204–6510	5691	(3ν_2, ν_2+ν_4+ν_6, ν_1+ν_2+ν_6)	[32]

4.1. 4800–5550 cm^{-1} and 8000–9200 cm^{-1}: prior Kitt Peak FTIR data

These two spectral intervals contain transitions of the lower Tetradecad and the Triacontad, correspondingly. As indicated previously in Table 6, no new studies were completed in the 4800–5550 cm^{-1} and 8000–9200 cm^{-1} intervals and so the prior lists from HITRAN2008 [10] were retained without modification. Both were based on measured positions and intensities retrieved from Kitt Peak FTIR spectra taken at room temperature using 0.011 cm^{-1} resolution [30]. Very few quantum assignments were available in both regions so most lower-state energies were set to 333.3333 cm^{-1}. We do note that part of the new parameters of the $2\nu_3$–ν_4 hot band [20] mentioned previously also extended up to 4870.6 cm^{-1}.

4.2. 5550–5855 cm^{-1}: Bruker FTIR (GOSAT) measurements

The prior HITRAN2008 line parameters from 5550 to 5855 cm^{-1} [10,30] were replaced by laboratory measurements obtained by GOSAT investigators [31 and the references therein]. The new measurements were based on spectra taken at 0.005 cm^{-1} resolution with Bruker 120 and 125 HR FT spectrometers using gas samples with temperatures between 180 and 296 K. Pressure broadening coefficients and their temperature dependences were also measured for specific transitions. This study reported a full list of measured line parameters from 5550 to 6236 cm^{-1}, but above 5855 cm^{-1}, more extensive work by other investigators appeared [32,33], as described below. As a result, only the lower part of the GOSAT 2009 line list below 5855 cm^{-1} was used without modification (i.e. merging with earlier results [30,34,35]).

4.3. 5855–7912 cm^{-1}: DAS and CRDS measurements

The list in the 5855.15–7918.94 cm^{-1} region was taken from very extensive experimental work performed in Grenoble to support planetary remote sensing. The positions and intensities were obtained from spectra recorded at 80 K and room temperature by differential absorption spectroscopy (DAS) in the strong absorption regions (the $2\nu_3$ region of the Tetradecad [36–40] and in the Icosad [41–44]) and high sensitivity CW-Cavity Ring Down Spectroscopy (CRDS) in the 1.58 μm [45–50] and 1.28 μm transparency windows [51]. The resulting **W**ang, **K**assi, **L**eshchishina, **M**ondelain, **C**ampargue (**WKLMC**) empirical lists for methane in "natural" abundance at 296 K and 80 K [32] were constructed for atmospheric and planetary applications, respectively. Transitions of the $^{13}CH_4$ and CH_3D isotopologues present in "natural" methane were identified by comparison with DAS spectra of "pure" $^{13}CH_4$ and CH_3D recorded at 80 K and 296 K. The upper panel of Fig. 3 shows the overview of the **WKLMC** list at 296 K where the $^{13}CH_4$ and CH_3D lines have been highlighted.

Empirical values of the lower state energy level, E_{emp}, of the transitions that appeared in both the 80 K and 296 K lists were derived by the so-called "two temperature (*2T*) method" i.e. from the ratio of the line intensities measured at 80 K and 296 K [51,52]. The "final" version of the

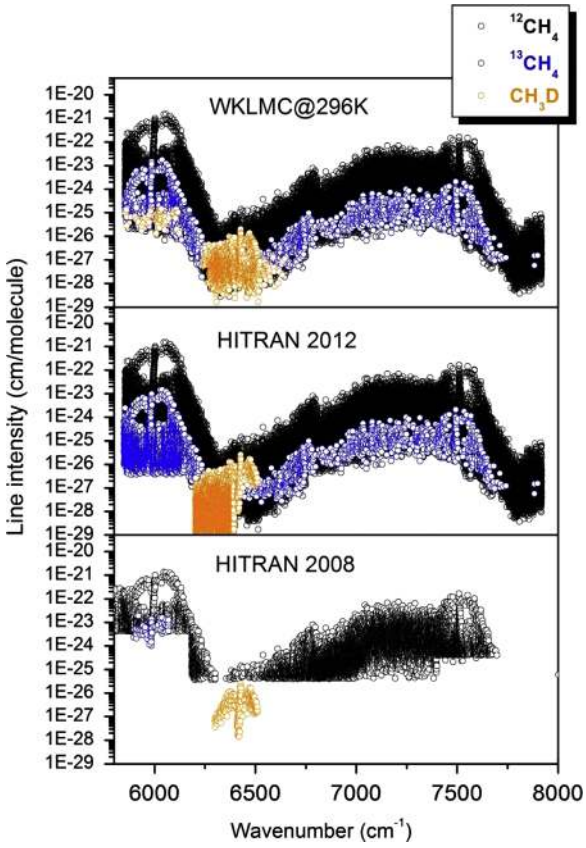

Fig. 3. Overview of the methane line lists (at 296 K) between 5855.15 and 7918.94 cm^{-1}. *From top to bottom*: WKLMC [32], HITRAN2012 [9], HITRAN2008 [10]. The black open circles correspond to the entire list with the initial assumption that they were $^{12}CH_4$ lines. Those later determined to be $^{13}CH_4$ and CH_3D transitions are highlighted in blue and orange, respectively. (To understand the use of color in this figure, please see the web version of this paper.)

WKLMC empirical lists for methane at 80 K and 296 K were recently released [32] by merging a previous version of the list [36] with new results obtained by DAS in the $2\nu_3$ region (5852–6183 cm^{-1}) [37].

Except for very accurate $^{12}CH_4$ frequencies from Zolot et al. [53] inserted for 112 positions of the $2\nu_3$ multiplets, the HITRAN2012 list in the 5855.15–7918.94 cm^{-1} region matches the positions and intensities in the **WKLMC** list at 296 K attached to Ref. [32].

In the HITRAN database, it is necessary to indicate the lines according to four different isotopologues ($^{12}CH_4$, $^{13}CH_4$, $^{12}CH_3D$ and $^{13}CH_3D$). This in fact is not always straightforward for empirical lists like **WKLMC**. Many studies initially use "normal sample" methane so that separate studies are required to understand the isotopic identity. An additional complication is that a small fraction of (generally weak) lines involve contributions of two or more isotopologues. In earlier forms of the **WKLMC** lists [36], they are marked $^{12}CH_4/^{13}CH_4$, $^{12}CH_4/CH_3D$ and $^{13}CH_4/CH_3D$, but there was insufficient analysis to know how much of the total absorption came from each species. Thus, a list obtained from spectra of highly enriched samples of the $^{13}CH_4$ and CH_3D minor isotopologues is

preferable to the incomplete line list extracted from the **WKLMC** list of natural methane.

The construction of the $^{13}CH_4$ and CH_3D list is described first, followed by details for $^{12}CH_4$.

4.3.1. $^{13}CH_4$

Between 5850 and 6150.00 cm^{-1}, the empirical list of $^{13}CH_4$ obtained by Fourier transform spectroscopy of "pure" $^{13}CH_4$ was adopted [54]. This list was partly rovibrationally "assigned" on the basis of the E_{emp} value obtained by the "2*T*-method".

Above 6150 cm^{-1}, no measurements of pure $^{13}CH_4$ were available, and so the $^{13}CH_4$ list was extracted from the **WKLMC** normal sample data; this is the only case where the **WKLMC** list was used for minor isotopologues. The resulting $^{13}CH_4$ list contained a number of E_{emp} values, but no assignments were available between 6150 and 7919 cm^{-1}. In the spectra recorded with natural methane, some $^{13}CH_4$ lines were obscured by stronger $^{12}CH_4$ absorption; consequently, the new HITRAN list of $^{13}CH_4$ above 6170 cm^{-1} is believed to be incomplete.

4.3.2. CH_3D

In spite of its low relative abundance, CH_3D contributes significantly to the (weak) absorption in the 1.58 μm window (6200–6500 cm^{-1}) in planetary spectra. Between 6305 and 6510 cm^{-1}, the HITRAN2008 list included only 271 lines of the $3\nu_2$ band centered at 6430 cm^{-1} and an unidentified band near 6425 cm^{-1} (34 lines) [55–57].

The new HITRAN list of CH_3D was extended to the 6204–6510 cm^{-1} region (see Fig. 4). It was constructed as follows:

- In the 6204–6394 cm^{-1} interval, the empirical list constructed in Lu et al. [52] by DAS of enriched CH_3D at 296 K was adopted. This work dedicated to the study of CH_3D at 296 K and 80 K in the $^{12}CH_4$ transparency window provided 5500 lines and 2723 E_{emp} values derived by the 2*T*-method. The new CH_3D list includes the assignment of the $3\nu_2$ lines as given in the HITRAN2008 list and about 175 additional assignments obtained by Ulenikov et al. [28] for the strongest lines. For the numerous other lines, the E_{emp} values are provided when available (about 2650 E_{emp} values in total).
- In the 6394–6510 cm^{-1} interval, the new CH_3D list is essentially the same as in HITRAN2008 and then limited to the $3\nu_2$ and 6425 cm^{-1} bands, except that a correction of a 2.0×10^{-3} cm^{-1} offset [52] in the HITRAN2008 positions was made.

Careful attention was paid to the normalization of line intensities for the abundances of CH_3D. In laboratory studies that use commercial natural methane, the abundance is different from that assumed in HITRAN compilations: 5.0×10^{-4} [47] from commercial supplies *versus* 6.15751×10^{-4} used for HITRAN2012 [9]. The included intensities were adjusted properly for the new CH_3D compilation.

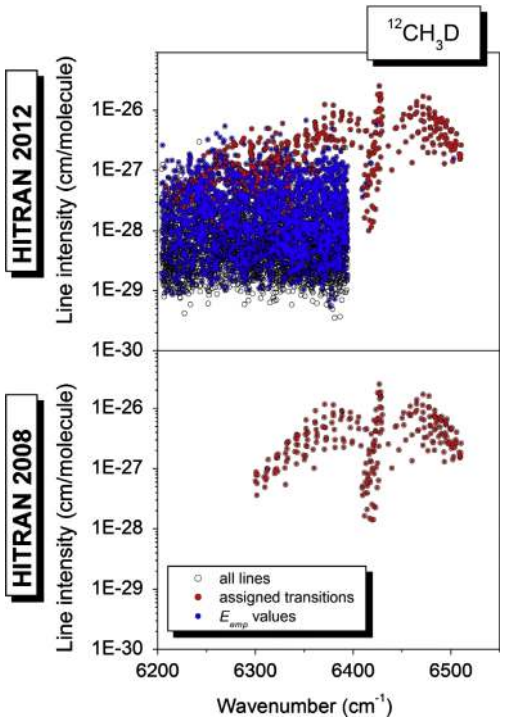

Fig. 4. Comparison of CH_3D from 6200 to 6550 cm^{-1} in HITRAN2012 and 2008. The gray open circles are observed intensities; solid red circles indicate those that are assigned from the theoretical analysis and solid blue circles show those that have empirical lower states. (To understand the use of color in this figure, please see the web version of this paper.)

4.3.3. $^{12}CH_4$

Following the construction of the $^{13}CH_4$ and CH_3D lists, in order to obtain the $^{12}CH_4$ list, all the $^{13}CH_4$ lines were removed from the **WKLMC** list together with all the CH_3D lines in the 6204–6394 cm^{-1} interval and the strongest CH_3D lines in the 6394–6510 cm^{-1} interval. All the other lines of the **WKLMC** list were then adopted for the $^{12}CH_4$ list. This is not fully satisfactory because the resulting list includes (i) a few CH_3D features identified below 6204 and above 6394 cm^{-1} which represents a small fraction of the CH_3D spectrum in the region (see Fig. 3), (ii) a few $^{12}CH_4/^{13}CH_4$ and $^{12}CH_4/CH_3D$ blended lines are labeled as $^{12}CH_4$ lines because the amount of absorption from $^{13}CH_4$ or CH_3D is not yet known. Consequently, in the regions where $^{13}CH_4$ or CH_3D lists were constructed from highly enriched spectra (below 6150 cm^{-1} for $^{13}CH_4$ and in the 6204–6394 cm^{-1} interval for CH_3D), the resulting "methane" absorption is expected to be slightly overestimated due to these $^{12}CH_4/^{13}CH_4$ and $^{12}CH_4/CH_3D$ blended lines which were kept in the $^{12}CH_4$ list. Nevertheless, this effect is very limited, and in absence of spectra obtained independently for the three methane isotopologues, the adopted procedure seems to be the best choice for the available empirical lists. The two lower panels of Fig. 3 comparing the list for "natural" methane in the 2008 and 2012 editions of the HITRAN database illustrate the important improvement concerning the minor isotopologues.

Contrary to the **WKLMC** lists [32,36] where the empirical E_{emp} values were preferred to insure a consistency between the line intensities at 296 K and 80 K, in the HITRAN list, the rovibrational assignments available in the literature were preferred to the E_{emp} values. The general strategy was then to attach the available rovibrational assignments to the **WKLMC** line parameters when the corresponding lower state energy value was consistent with E_{emp} values. More precisely, the line intensity at 80 K was computed using the lower state energy value obtained from the rovibrational assignment and comparing it to its value measured at 80 K (as included in the **WKLMC** list at 80 K [32]). This procedure proved very efficient in detecting erroneous assignments [33].

In two intervals, rovibrational assignments were available for $^{12}CH_4$ from only three sources:

- **Between 5855 and 6204.6 cm^{-1}**, the GOSAT empirical list [31] provided ~2000 rovibrational assignments. About 200 of them were found in strong contradiction with the T dependence of the measured line intensity [33] and so the assignment was rejected (i.e. the E_{emp} value was preferred when available).
- **In the 6350-6500 cm^{-1} interval** corresponding to the $5\nu_4$ and $\nu_2+4\nu_4$ bands in the Icosad system, Nikitin et al. [48] used the effective operator approach to compute a theoretical line list which reproduces satisfactorily the CRDS spectrum in the region. Some assignments were also provided for the surrounding regions from Reims FTS spectra recorded with a path length of 1800 m. In the new HITRAN list, the assignments were attached to the **WKLMC** lines by visual comparison with a theoretical spectrum [48]. If we noted large deviations between the calculations and the **WKLMC** empirical list, E_{emp} values were preferred when available. In addition, in two intervals (6256–6350 cm^{-1} and 6500–6550 cm^{-1}), some additional assignments and lower state energies from Ref. [48] were inserted.
- Finally, the HITRAN2008 list included 76 lines assigned to the $\nu_2+2\nu_3$ band near 7510 cm^{-1}. All but three of them were confirmed by the T dependence of the intensities and were transferred to the new list; Fig. 9 of Ref. [41] shows an example of erroneous assignment which was not transferred. Additional identifications were checked and completed using revised assignments from pulsed supersonic jet CRD spectroscopy of Manca Tanner and Quack [58], which updated and complemented earlier work with this technique [59].

The lines left without assignments or E_{emp} values were those observed only at 296 K but not at 80 K. As a rule, they corresponded to hot-band transitions (from the ν_2 and ν_4 bending levels of $^{12}CH_4$ at 1583 and 1367 cm^{-1}, respectively) and high-J lines whose intensities at 80 K became too small to be detected in the cold spectra. An artificial (default) value of 999.999 cm^{-1} was attached to such $^{12}CH_4$ lines.

It is worth emphasizing that for planetary atmospheres applications at low temperature (typically Titan), the **WKLMC** list at 80 K attached to Ref. [32] is better than the new HITRAN list extrapolated from 296 K to 80 K; the 80 K list has lines missing from the HITRAN list at 296 K, but their intensities cannot be normalized to 296 K without knowledge of the lower state energy. The **WKLMC** list at 80 K was successfully applied to simulations of Titan spectra at different resolutions taken from the ground or by the DISR instrument on board the Huygens probe [3,60,61] and to spectra of Pluto [62], Uranus [63], Saturn and Jupiter [64].

The comparison of the 2008 and 2012 HITRAN lists of $^{12}CH_4$ and $^{13}CH_4$ presented in Fig. 5 emphasizes improvements for weak lines in the planetary "transparency" windows (1.58 μm and 1.28 μm). Many rovibrational assignments or E_{emp} values are now known so that the temperature dependence of intensities can be computed; this was not possible with the earlier measurements [30].

As seen in Table 10, the known rovibrational assignments in the $2\nu_3$ (1.66 μm) and $5\nu_4,\nu_2+2\nu_3$ (1.4 μm) regions correspond to ~8.5% of the total number of lines, but they represent ~65% of the total intensity. 38% of the lines are given with E_{emp} values and contribute 28% of the total intensity. In contrast, the large set of the remaining lines (53%) represents only 6.7% intensity at room temperature.

4.4. 10,923–11,502 cm^{-1}: ICLS

This spectral region contains transitions of the Pentacontakaipentad (polyad P_8 in Fig. 1), and its line-by-line parameters [65] appear for the first time in the HITRAN database. These line parameters were determined from analysis of spectra obtained using the intracavity laser spectrometer (ICLS) at the University of Missouri at St. Louis [66]. Methane spectra at low temperature (99–161 K), low pressure (0.12–7.13 Torr), long path (3.14–5.65 km) and high resolution (~0.01 cm^{-1}) were obtained for the entire 890 nm band (10,925–11,500 cm^{-1}). At these cold temperatures, the Doppler width is 0.01 cm^{-1} and the spectral lines originating from levels higher than $J''=11$ and excited vibrational states are not visible. The result is a dense, but manageable spectrum from which over 11,200 line positions, intensities and lower state energies are derived on a line-by-line basis using the College of William and Mary multispectrum nonlinear least squares fitting program [67].

5. Pressure broadening and shift parameters

There are currently only ~7000 total individual measured half width coefficients for $^{12}CH_4$ and $^{13}CH_4$ (see [68–76] and references cited therein). This total count includes broadening by CH_4 (self), air, N_2, O_2, H_2, He, Ne, Ar and Xe, and also transitions measured by more than one study. Even fewer studies report measured pressure-induced shifts and temperature dependence exponents for widths. These measured data fall well short of the number needed to have accurate broadening and shift parameters for the 409,000 lines of the first two isotopologues in the new methane compilation. In the measured data it is difficult to discern systematic patterns of variation of the widths and shifts with vibrational and rotational quantum numbers, other than a general trend for

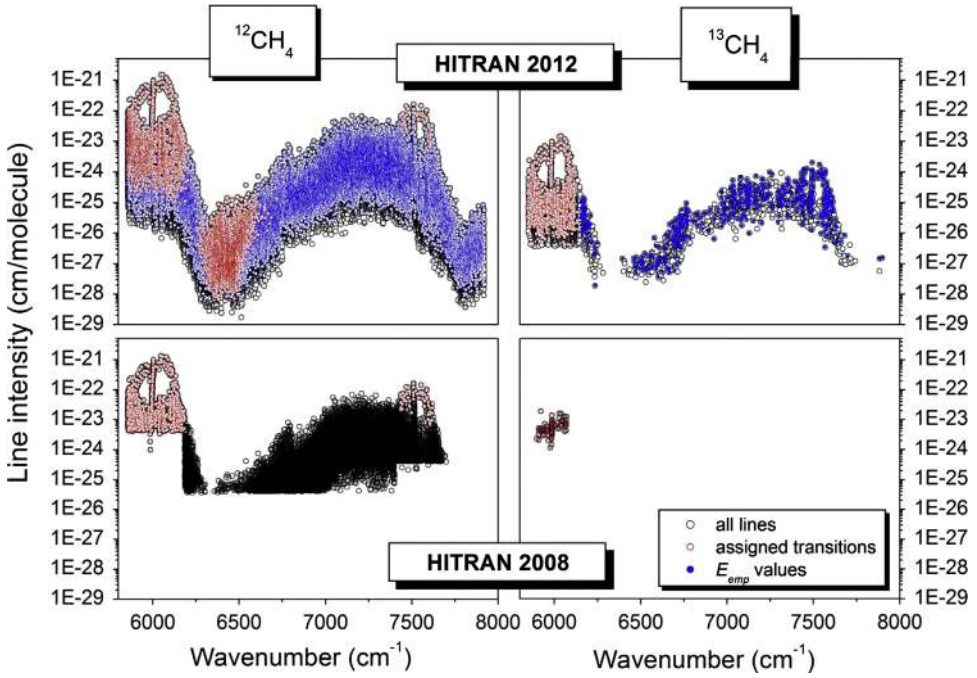

Fig. 5. Overview of $^{12}CH_4$ and $^{13}CH_4$ between 5855.15 and 7918.94 cm^{-1} in HITRAN2008 and HITRAN2012. The lines with rovibrational assignments and with empirical lower state energies are highlighted in red and blue, respectively. (To understand the use of color in this figure, please see the web version of this paper.)

Table 10
Summary of the new $^{12}CH_4$, $^{13}CH_4$ and CH_3D parameters from 5855.15 to 7918.94 cm^{-1}the number of lines, assignments and observed empirical lower state energies.

	$^{12}CH_4$	$^{13}CH_4$	CH_3D
Numbers by lower state energies			
Assignments	4464	1082	377
E_{emp}	20,075	613	2533
No E_{emp}	27,766	2990	2782
Total	**52,305**	**4685**	**5692**
Sum of intensities (in 10^{-20} cm^{-1}/(molecule cm^{-2}) at 296 K) (and percentage of the total list)			
Assignments	8.69 (65.0%)	7.19×10^{-2} (72.3%)	1.29×10^{-4} (52.6%)
E_{emp}	3.78 (28.3%)	9.6×10^{-3} (9.6%)	8.94×10^{-5} (36.6%)
No E_{emp}	9.01×10^{-1} (6.7%)	1.80×10^{-2} (18.1%)	2.66×10^{-5} (10.9%)
Total	**13.4**	**9.95×10^{-2}**	**2.45×10^{-4}**

the widths to decrease with increasing J. Several studies have also noted that for the same J, the E species transitions usually have smaller half widths relative to A or F species transitions. Some similarities in the width and shift patterns between bands have been noted, for example, between ν_4 and $\nu_1+\nu_4$, or between ν_3 and $2\nu_3$. The available recent nitrogen broadening calculations [77,78] are in reasonable agreement (5–15%) with measurements for the fundamental bands, but systematic offsets between observed and calculated widths are also seen for the higher vibration–rotation bands [74–76 and the references therein].

The situation for the 59,000 lines of the two CH_3D isotopologues is somewhat similar. Except for the one study in the $3\nu_2$ region [79], empirical width and shift coefficients for some 2000 individual transitions are reported for only the four lowest fundamentals [80–89]. Empirical expressions as a function of the quantum numbers are available based on measurements in the triad region [80–85] to approximately represent the air-, N_2-, and self-broadened halfwidths and pressure-induced shifts of unmeasured transitions.

For $^{12}CH_4$ and $^{13}CH_4$ lines, widths and temperature dependence coefficients from different sources were inserted. Some were direct measurements of air (or N_2) and self broadening from the literature, some were predictions from theory [68]. but most were estimated using values shown in Table 11 (similar to those applied previously [90,91]). Below 4800 cm^{-1}, the list was comprised of predictions in which lower-state J was always explicitly

Table 11
Estimated broadening coefficients as a function of J''.

$J''=$	0	1	2	3	4	5	6	7	8	9	10
Air widths[a]	0.060	0.065	0.065	0.066	0.065	0.063	0.061	0.060	0.058	0.055	0.054
$J''+10$		0.052	0.052	0.049	0.049	0.048	0.048	0.049	0.049	0.047	0.046
$J''+20$		0.045	0.044	0.043	0.042	0.041					
Self γ widths[a]	0.081	0.081	0.082	0.079	0.078	0.077	0.077	0.076	0.074	0.073	0.070
$J''+10$		0.068	0.067	0.065	0.065	0.063	0.061	0.060	0.059	0.058	0.058
$J''+20$		0.057	0.057	0.056	0.056	0.055					
Temp dep[a]	0.65	0.68	0.70	0.73	0.72	0.72	0.70	0.70	0.69	0.65	0.64
$J''+10$		0.64	0.63	0.63	0.62	0.62	0.61	0.61	0.60	0.60	0.59
$J''+20$		0.59	0.58	0.58	0.57	0.57					

[a] Broadened width coefficients are in units of cm^{-1}/atm at 296 K. Temp dep is the temperature dependence exponent tdep for $\gamma_T=\gamma_{296\ K}\ [296/T]^{tdep}$; pressure shifts for air are assumed to be shift = position $\times -2.0\times10^{-6}$ cm^{-1}.

Table 12
HITRAN integer codes to indicate accuracies of line parameters.

Parameter↓	**Code→**					
	1	**2**	**3**	**4**	**5**	**6, 7**
Position and shift (cm^{-1})	0.1–1.0	0.01–0.1	0.001–0.01	0.0001–0.001	0.00001–0.0001	<0.00001
% Intensity broadening	Default constant	Estimate	20	10–20	5–10	2–5, 1–2

Table 13
Example of accuracy codes for $^{12}CH_4$ Pentad transitions.

Band	**Position**[a]	**Intensity**[a]	**HITRAN**[b]		**Assignment**		**Codes**		
			Upper	**Vib**	$J'C'\alpha'$	$J''C''\alpha''$	ν	s	γ
$2\nu_2$	2998.566351	4.020E−22	0 2 0 0	1E	6F2 30	7F1 2	**4**	**5**	**4**
$2\nu_2$	2996.272904	3.266E−23	0 2 0 0	1A1	6F2 29	7F1 1	**4**	**4**	**4**
ν_3	2948.421423	5.149E−20	0 0 1 0	1F2	6F1 25	7F2 1	**7**	**6**	**5**
ν_1	2843.727752	1.285E−24	1 0 0 0	1A1	6F2 22	7F1 1	**3**	**4**	**4**
$\nu_2+\nu_4$	2823.468689	1.929E−21	0 1 0 1	1F2	6F1 13	6F2 1	**4**	**6**	**5**
$\nu_2+\nu_4$	2803.858837	1.260E−21	0 1 0 1	1F1	6F2 13	6F1 1	**4**	**6**	**4**
$2\nu_4$	2561.382113	4.237E−23	0 0 0 2	1E	6F1 7	7F2 1	**4**	**4**	**4**
$2\nu_4$	2509.438662	3.276E−25	0 0 0 2	1A1	6F1 3	7F2 1	**3**	**3**	**4**
$2\nu_4$	2473.590124	1.957E−22	0 0 0 2	1F2	6F1 7	7F2 1	**3**	**3**	**4**

[a] The units are, for columns two and three respectively, cm^{-1} and cm^{-1}/(molecule cm^{-2}) at 296 K.
[b] The vibration lower state of these transitions is 0 0 0 0 1A1; in the last column ν, s *and* γ stand for positions, intensities and air-broadened widths, respectively.

written. Above 4800 cm^{-1}, some of the entries were given either with partial assignments or with empirical lower-state energies; the latter were used to estimate the lower-state J so that broadening coefficients in Table 11 could be inserted.

As done previously [10], if no direct measurements were available, the air-broadened pressure shift coefficients were set using a multiplying factor of -2×10^{-6} times the value of the line position [27]. It is hoped that the width values have at least 20% accuracy for the majority of the lines, but the uncertainty for the shift estimate is unknown.

Below 4800 cm^{-1}, some broadening coefficients were retained from the HITRAN2008 list; this included the predicted widths of ν_3 A and F lines [68] as well as earlier measurements of the Dyad, Pentad and Octad [70–74]. In the far-IR, newly-measured N_2- and self-broadened widths of GS–GS and Dyad–Dyad transitions (mostly the ν_4–ν_4 hot band) were inserted as well [69]. Above 5500 cm^{-1}, measured air- and self-widths, temperature dependence coefficients and air pressure shifts [75,76] were transferred from the GOSAT compilation [31] into the new HITRAN list.

6. Accuracies and caveats

The ranges of accuracy codes shown in Table 12 were applied to the line parameters. Those for positions and intensities that came directly from measurements were estimated line-by-line by the investigators, but it was difficult to give reliable accuracy codes for all the *predicted* positions and intensities.

An illustration of the accuracy codes is shown in Table 13 using selected transitions of the $^{12}CH_4$ Pentad taken from HITRAN2012. This polyad has five different vibrational bands ($2\nu_2$, ν_3, ν_1, $\nu_2+\nu_4$ and $2\nu_4$), but there are nine *sub-vibrational* levels because three states have multiple components. In principle, if no ro-vibrational interactions were possible between these nine components, only the three F2 levels would produce infrared absorptions. Instead, all nine components contribute transitions to the Pentad region (2200–3300 cm^{-1}). If measured positions and intensities of these states were not directly modeled, their accuracies are much less certain.

In general, if measured transitions were well reproduced by theoretical modeling, the positions and intensities were given good uncertainty codes (3 and 4 for positions; 5 and 6 for intensities); the use of "7" (e. g. for the transition at 2948.421423 cm^{-1}) indicates that the original predicted position was replaced by the sub-Doppler measurement [19]. However, a poorer accuracy was assumed for *weak transitions* whose intensities are less than two orders of magnitude compared to the strongest lines in the same polyad. In general, the uncertainty codes for bands from the ground state to the Dyad and Pentad levels are more reliable through the range of *J* values included in the model (see Tables 2 and 3). However, it was difficult to characterize the real accuracies of some predicted Octad levels and also the intensities of most hot bands.

We emphasize that all prior FTIR measurements from 5550 to 5855 cm^{-1} and 5855 to 6205 cm^{-1} [30] were replaced with new results from two specific studies [31,32] shown in Fig. 6. These changes correct many of the prior inadequacies of missing lines and unknown lower state energies which are important for planetary remote sensing. However, there was no effort to combine results from other individual studies [35–37,92–95]. Further research is currently in progress, and the results from prior and new studies will be merged at the first opportunity to provide an interim update posted online at the HITRAN website.

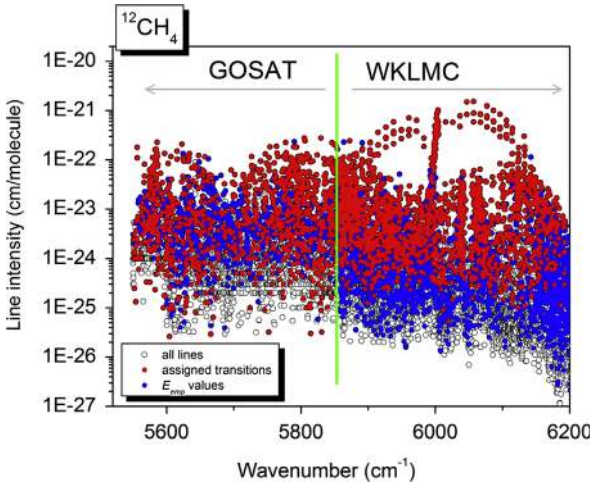

Fig. 6. Data sources in the upper Tetradecad region. Open circles are observed intensities at 296 K; solid red circles indicate those assigned by theoretical analyses, and solid blue circles show those with empirical lower states. (To understand the use of color in this figure, please see the web version of this paper.)

The list does not provide all possible or needed improvements for this upper Tetradecad region. The present goal for observed positions is 0.001 cm^{-1} and 3% for measured intensities at room temperature for the stronger lines, but accuracies of some weaker features will be worse for the reasons discussed in Section 4. In any list of measurements, part of the observed absorption can be due to more than one transition; therefore it should not be assumed that all the measured intensity arises from the assignments listed. The observed empirical lower state energy can provide some clues, but there is no place to include the estimated accuracies for these parameters. However, such details are provided in the original papers.

7. Prospects for future improvement

7.1. Analyses and effective Hamiltonians for higher polyads

As seen in Table 10, there are over 60,000 measured features of the three isotopologues compiled from 5850 to 7912 cm^{-1} but less than 10% have *confirmed* quantum assignments. The difficulties in improving this situation quickly are demonstrated in Table 14 which lists nine polyads and their spectral ranges along with the number of nominal bands in each level. The remaining columns (A_1, A_2, E, F_1, F_2) show the total number of "sub-vibrational" states with a breakdown according to vibrational symmetry. If all the F_2 vibrational components could not share intensity with the other four A_1, A_2, E, and F_1 vibrational levels, the methane spectrum up through Polyad 8 could be modeled by considering less than 650 F2 states, instead of over 2000 sub vibrational levels.

Even in the most recent Tetradecad study [6], assignments are known for only about 25% of the 60 subvibrational levels of $^{12}CH_4$. As described previously, there is a huge amount of experimental FTIR, CRDS, ICLS etc. data already available. Future analyses and theoretical modeling can greatly improve the methane database in the near-IR, especially for the Icosad. For the Triacontad and Tetracontad polyads, a similar set of measurements at cold temperatures is needed before much progress can be expected, however. One cannot expect to have reliable predictions sufficient for accurate Earth remote sensing (see Table 1) without better theoretical models that reproduce the experimental precisions and absolute accuracies of state-of-the-art laboratory measurements.

7.2. Theoretical studies and recent ab initio results

Much progress was recently achieved in *ab initio* calculations for methane [96–111]. Marquardt and Quack provided the first global potential hypersurfaces for the spectroscopy and dynamics of methane based on *ab initio* calculations [96,97]. Schwenke and Partridge [98,99] carefully investigated the role of various approximations in electronic structure calculations to the methane potential energy surface (PES) which was used by Wang and Carrington [100] to test an internal coordinate variational method that makes it possible to calculate high-*J* rovibrational levels of excited

Table 14
Summary of the number of methane vibrational states.

Methane polyads[a]		Range (cm^{-1})	# Vib levels[b]	# Sub-vibs[c]	# Sub-vib levels by symmetry species[d]				
Index	Name				A_1	A_2	E	F_1	F_2
P_0	Monad (i.e. G.S.)	0	1	1	1	0	0	0	0
P_1	Dyad	1300–1500	2	2	0	0	1	0	1
P_2	Pentad	2600–3100	5	9	3	0	2	1	3
P_3	Octad	3900–4600	8	24	4	2	5	5	8
P_4	Tetradecad	5200–6200	14	60	11	2	14	13	20
P_5	Icosad	6500–7700	20	134	18	11	28	34	43
P_6	Triacontad	7800–9300	30	280	41	20	58	71	90
P_7	Tetracontad	9100–10800	40	538	64	45	112	148	169
P_8	Pentacontakaipentad	10,400–12300	55	996	126	81	204	272	313

[a] The vibrational polyads P_n of methane as defined by a *polyad quantum number*. $n=2v_1+v_2+2v_3+v_4$ where v_i is vibrational quantum number related to the fundamentals.
[b] Total number of vibrational levels involving quanta of the four fundamentals (ν_1, ν_2, ν_3, ν_4).
[c] Number of vibrational sub-levels within each polyad.
[d] Number of vibrational sub-levels within each polyad according to vibrational symmetry.

vibrational states. Yurchenko et al. [101] applied *ab initio* techniques to determine relative signs of the electric dipole moments and then estimate methane vibrational band strengths up to 10,000 cm^{-1}.

The most accurate up-to-date methane PES in the spectroscopically accessible range is the recent NRT (Nikitin, Rey and Tyuterev) surface [102] based on extended *ab initio* calculations on 19,882 nuclear configurations up to 20,000 cm^{-1} with a subsequent empirical optimization using 4-parameter scaling to fundamental frequencies. These authors have also calculated the *ab initio* dipole moment surface (DMS) [103] for the same number of points. These surfaces will be referred to as NRT PES and DMS. A new *ab initio* equilibrium configuration Re = 1.08601 ± 0.00004 Å [102] permitted the pure rotational (GS) levels to be calculated from this PES with an average accuracy of 10^{-3} cm^{-1} or better for transitions up to $J=20$ [103,104,106]. This latter result was checked with independent methods [105], and the rms deviation for band centers was 0.08 cm^{-1} up to the Pentad, 0.25 cm^{-1} up to the Octad, ~1 cm^{-1} for the Tetradecad [102] and ~1–2 cm^{-1} for the experimentally known Icosad bands [106].

The absolute accuracy of the far-IR intensities still requires further study. Cassam-Chenai and Liévin [23] computed rotational GS–GS Q and R branch transitions from NRT PES using perturbation methods; their *ab initio* DMS was calculated with higher cardinal number of the electronic basis, but at smaller set of ~100 points. Their calculations were closer in average to recent experimental intensity measurements [18] than to HITRAN2008 data, although a significant scatter for individual line intensities gave a rms deviation of 6%. Variational calculations from *ab initio* NRT DMS [103,104] gave slightly lower intensity values than those of HITRAN2008 by 2–5% in integrated GS–GS band intensity with very smooth deviations and rms (calc.—HITRAN2008) of ~3%. For infrared bands, the agreement of first-principle variational predictions reported by Nikitin et al. [103] and Rey et al. [104,108] with HITRAN2008+GOSAT data using the cut-off $J_{max}=25$ was the following: 4% for the Dyad, 2.5% for the Pentad, 1.5% for the Octad, 6% for the Tetradecad and 3% for the Icosad. *Ab initio* predictions from the NRT DMS also gave an excellent agreement with the recent experimental line list of Grenoble [32] at 80 K: the discrepancy was only 2% for integrated intensity in the entire Icosad range 6300–7800 cm^{-1} [108]. The rms deviation at $T=296$ K for strong and medium line intensities for low J values was 3–5% for the Dyad, Pentad and Octad [104,108]. For higher ranges 8000–9300 cm^{-1} (Triacontad) and for weak transitions the agreement was qualitatively reasonable [102,108]. In total, about 1.5 million lines of $^{12}CH_4$ and $^{13}CH_4$ at room temperature have been generated [104,108] up to 9300 cm^{-1}. Assigning and modeling all the measured spectral features remain a formidable challenge for the theory.

Successful *ab initio* predictions will be particularly important for exoplanet studies. All the remote sensing applications indicated in Table 1 require reliable methane compilations up to at least 7700 cm^{-1}, but the contributions from hot bands are essential for the high temperature applications (e.g. exoplanet, brown dwarfs and combustion studies). For instance at 1200 K, only 52% of the methane molecules are in the vibrational ground state. As discussed by Borysov et al. [109] and illustrated in Fig. 7, the absorption from the two strongest sets of hot bands have intensity nearly equal to that arising from the Pentad–GS bands even at modest hot temperatures between 1000 and 1300 K. Such hot bands will dominate hot CH_4 spectra at even higher temperatures. Of course, some methane hot bands arising from the Dyad as the lower state do appear in spectral observations of cold outer planets and moons if the abundances are sufficiently high.

In any case, the number of individual transitions associated with hot bands up through 10,000 cm^{-1} is tremendous (hence the large estimate in Table 1 for exoplanets). Unfortunately, as seen in Table 2, effective Hamiltonian calculations are currently limited to the already modeled vibrational states. i.e. the Tetradecad and below. No hot bands that fall within the Tetradecad region *can be reliably predicted without a better understanding of the Icosad and the higher polyads*. New research for the Octad [4] does provide predictions of the Octad–Dyad line positions, but some of

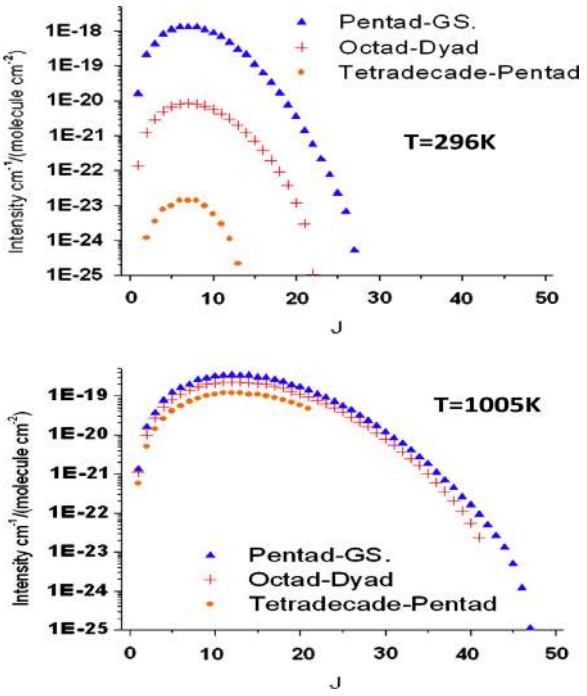

Fig. 7. The effect of gas temperatures on methane absorption at 3.3 μm. Calculated intensities as a function of J are shown at 296 K (upper panel) and 1005 K (lower panel) for the five Pentad bands arising from the ground state (▲), 16 hot bands for the Octad–Dyad (+) and 540 possible hot bands of the Tetradecad–Pentad (•) [106]. The intensities are given in units of $cm^{-1}/(molecule\ cm^{-2})$ at the given temperature.

the computed intensities need adjustments and have not been used for HITRAN2012.

A first step toward substantial improvements in high-energy ranges would be to consider *ab initio* predictions as a starting point for improvements of spectroscopic models. Niederer et al. [7] demonstrated that accurate predictions for rovibrational levels and $^{12}C/^{13}C$ isotope shifts can be obtained from empirically adjusted potentials based on *ab initio* calculations. The theoretical rovibrational levels can be successfully fitted by the Dijon effective Hamiltonian model [111] leading to better prediction and analysis of experimental data. As shown by Tyuterev et al. [106], effective polyad Hamiltonians can be computed from the recent *ab initio* PES [102] with an average error in predicted band centers of ~1–2 cm^{-1} for all experimentally known bands up to the Icosad range. Accurate predictions of ro-vibrational coupling parameters were found particularly important for a reliable description of the resonance perturbations and intensity transfer between strong and weak bands [106,108]. As both *ab initio* and effective models can now be converted in the same symmetry-adapted tensorial formalism [107,110], this supplementary information would help better characterization of poorly fitted parameters, allow more robust predictions for high-J states and open the door for further line-by-line analyses that are otherwise intractable. Note that a good agreement for integrated intensity of the hot bands (though only compared at room temperature) in Refs. [104,108] suggests that *ab initio* calculations could be extended to high temperatures. Predictions for high-temperature spectra are currently under way (e.g. Refs. [101,106,108]).

7.3. Future needs for pressure broadened line shapes

Methane features are utilized from the far-infrared into the visible to discern physical and chemical properties of atmospheres. A wide range of remote sensing applications rely on Voigt line shapes and request better characterization of the basic set of broadening parameters (Lorentz widths, pressure-induced shifts and *the corresponding temperature dependences*) in order to meet their specific accuracy requirements (see Table 1). Unfortunately, many laboratory measurements involve only lower vibrational bands so that the vibrational and rotational dependence of the broadening coefficients remains largely unknown for transitions in the near-IR. As summarized by Tables 2 and 3 of Ref. [68] and the more recent experimental work described in Section 5 of the present paper, the numbers of laboratory-measured values of line widths (a few thousands), shifts (less than a thousand), and mixing parameters (a few hundred), as well as their temperature dependences (less than a thousand), remain small compared to the 468,000 transitions now given in HITRAN2012.

This lack of knowledge hinders some techniques used to characterize atmospheric molecules. For example, Brogi et al. [112] detected H_2O and CO at 2.3 μm by applying *sensitive cross-correlation* to relatively high resolution (~0.04 cm^{-1}) spectral observations of a distant exoplanet. The current absolute accuracies of line positions needed for this usage is at least 0.002 cm^{-1}, but the pressure-induced shifts (assumed to be arising from hot H_2) as a function of temperature are largely unmeasured in the near-IR.

To provide accurate shifts and the other parameters required, it is necessary to discern systematic patterns in the measured methane broadening coefficients as a function of the vibrational and rotational quantum numbers (J, C, α). The widths do decrease with increasing J; in the infrared-active fundamentals, the E species transitions often have smaller half widths compared to A or F species transitions and also vary with the value of "α". However, patterns are not clear enough in near-IR bands to develop simple empirical expressions as a function of the rotational quanta, as has been done for CH_3D [79–84].

The best hope for increased understanding is through theoretical prediction from quantum mechanics with validation by extensive experimental results. Recent modeling efforts [77–78] are able to reproduce some $^{12}CH_4$ laboratory measurements of N_2-broadened widths within ±5–15%. Modeling efforts are ongoing to improve the accuracies of line broadening and shift calculations in the Dyad and Pentad regions, particularly for the temperature dependences, but the long-range prospect for much needed improvement at the near-infrared wavelengths (see Fig. 6 of Ref. [77]) is uncertain unless such studies receive financial support.

While 5% accuracy may often be sufficient for many planetary studies, higher accuracy requirements (0.5–1%) for Earth remote-sensing measurements [2] will require

inclusion of some "non-Voigt" line shapes such as line mixing, speed dependence and collisional narrowing, characterized as a function of temperature [113–115]. Unfortunately, laboratory measurements of methane line mixing for terrestrial atmospheric conditions are sparse [70–76,114,116–118] and most involve the lower polyads: ν_4, ν_2, ν_3, $\nu_2+\nu_3$ of $^{12}CH_4$ and ν_4 of $^{13}CH_4$ [72]. These relatively few studies permit rather limited comparisons of measured line mixing parameters between different bands and between the two isotopologues [70–73]. Laboratory studies of speed dependence or collisional narrowing for methane transitions (e.g., [114,116–118]) are available for only a small number of lines.

Eventually, non-Voigt line shape parameters for methane transitions must be included in the HITRAN database, but more study is needed. A decade ago, a review of pressure broadening concluded that some non-Voigt line shapes for remote sensing of methane were needed [91], but there was insufficient information to include these coefficients in the HITRAN database. Since then, software codes developed to model line mixing for atmospheric methane retrievals in the ν_4, ν_3, and $2\nu_3$ regions [92,115,119,120] have become available to atmospheric remote-sensing users. The structure of the HITRAN database is being changed to add such important parameters in the future [121,122]. However, additional experimental, theoretical, and observational studies of pressure broadened methane in near infrared bands must be performed to understand which line shape formulations are needed to meet state-of-the-art remote sensing requirements for the atmospheres of Earth, solar system planets, and exoplanets. With sufficient number and adequate wavelength coverage, these new measurements and observations can be used to develop and validate theoretical models to accurately calculate the required methane line shape parameters *as a function of temperature* for the important planetary broadeners (N_2, O_2, H_2, He).

8. Conclusions

Recent advances in understanding the spectrum of methane provided this major update of the methane line parameters for remote sensing. The resulting compilation is now included in HITRAN2012 [9]. Theoretical modeling, combined with extensive new laboratory measurements, permitted many more line positions, intensities and lower state energies to be included. Continued analyses of the measured positions and intensities are needed to provide good model predictions for the near-IR polyads now represented by measured values.

One remaining major shortfall is poor accuracies for the pressure-broadened line shape parameters applied throughout the database. New research must be pursued to extend both the measurements and theoretical predictions of CH_4 broadened by N_2, H_2, He, O_2 etc. throughout the infrared. To meet the high accuracy requirements of Earth remote sensing, new studies must also investigate non-Voigt line shape models within the important near-IR bands.

The precise knowledge of the methane absorption in the study of planetary (and exoplanetary) objects is vital because the information inferred on the physical properties from the modeling of any available data is extremely dependent on this information. In the case of our own planet's atmosphere, where CH_4 is a major greenhouse gas, current studies aiming to map its sources and sinks with satellite missions (like GOSAT) or the applications in industrial studies of the environment or as a fuel, are based on a good understanding of the methane spectroscopy. Another important example is Titan (Saturn's largest satellite), whose atmosphere is mainly composed of nitrogen and methane, and where CH_4 is again a major greenhouse gas and the main atmospheric absorbing constituent in the near-infrared. Titan has been continuously explored by the Cassini–Huygens mission since July 2004 and is planned to remain until 2017. The accurate simulation of the methane contribution in the analysis of such space data, as well as of ground-based observations, allows scientists to correctly characterize the satellite's atmosphere and surface. Indeed, in the absence of reliable absorption coefficients for methane in the specific Titan's conditions (low temperatures, long path lengths) in the near infrared (especially between 0.8 and 2 μm), the scientific community continually faces the difficulty of analyzing the high-quality spectra and images collected at these wavelengths. The new database will remedy this problem and considerably reduce the uncertainties in the results. Defining the chemical atmospheric composition and the nature of the surface of this satellite gives access to important physical, geophysical, meteorological and astrobiological aspects in the formation and evolution of our solar system and of our own planet, because conditions prevailing on the primitive Earth are expected to be similar to those in Titan today. Understanding the methane contribution is also essential in the studies of other planetary objects like Saturn, Uranus, Neptune, and Pluto, where the methane abundance in the gaseous atmosphere is significant. For Saturn in particular the accurate description of the methane content gives access to the vertical structure and to the mapping of the planet's haze from Cassini data. At the other end of the temperature range, the methane description at high temperatures is necessary for the study of exoplanets, a new evolving field with great importance in astrophysical studies.

Acknowledgments

The authors wish to thank the many sources of funding and technical support that made this advancement possible.

This work is part of the ANR Project "CH4@Titan" (Ref: BLAN08-2_321467). The international funding support includes the LEFE-Chat CNRS French grant and the Groupement de Recherche International SAMIA between CNRS (France) and RFBR (Russia), Program Number 22: the fundamental problems of investigation and exploration of the Solar System of Russian Academia of Science; Grant in Aid for Scientific Research (A) and the Photon Frontier Network Program of the Ministry of Education, Culture,

Sports, Science and Technology in Japan; the Swiss National Science Foundation, ETH Zurich; the Natural Sciences and Engineering Research Council of Canada, the Canadian Space Agency and CAS (China). We are grateful for the support from IDRIS/CINES computer centers of France and also the computer center Reims-Champagne-Ardenne.

Part of the research at the College of William and Mary, Connecticut College, Langley Research Center, the Harvard-Smithsonian Center for Astrophysics and the Jet Propulsion Laboratory (JPL) was performed under contract with National Aeronautics and Space Administration. Funding for research at Bridgewater College was provided by the Martin Summer Science Research Institute and from an American Astronomical Society Small Research Grant.

References

[1] Tinetti G, Deroo P, Swain MR, Griffith CA, Vasisht G, Brown LR, et al. probing the terminator region atmosphere of the hot-JUPITER XO-1b with transmission spectroscopy. Astrophys J Lett 2010;712:L139–42.

[2] ESA Climate Change Initiative (CCI) User Requirements Document Version 1 (URDv1) for the Essential Climate Variable (ECV) Greenhouse Gases (GHG); 2011. p. 19. ⟨http://www.esa-ghg-cci.org/?q=node/95⟩.

[3] Atkinson DH, Kazemineja B, Gabori V, Ferri F, Lebreton J-P. Huygens probe entry and descent trajectory analysis and reconstruction techniques. Planet Space Sci 2005;53:586–93.

[4] Daumont L, Nikitin AV, Thomas X, Régalia L, Von der Heyden P, Tyuterev VlG, et al. New assignments in the 2 μm transparency window of the $^{12}CH_4$ Octad band system. J Quant Spectrosc Radiat Transfer 2013;113:101–9.

[5] Albert S, Bauerecker A, Boudon V, Brown LR, Champion JP, Loëte M, et al. Global frequency and intensity analysis of $^{12}CH_4$ in the 0–4800 cm^{-1} region. Chem Phys 2009;356:131–46.

[6] Nikitin A, Boudon V, Wenger C, Albert S, Brown LR, Bauerecker S, et al. High resolution spectroscopy and first global analysis of the Tetradecad region of methane $^{12}CH_4$. Phys Chem Chem Phys 2013;15:10071–93. http://dx.doi.org/10.1039/C3CP50799H.

[7] Niederer HM, Wang X-G, Carrington Jr. T, Albert S, Bauerecker S, Boudon V, et al. Analysis of the rovibrational spectrum of methane $^{13}CH_4$ in the Octad range. J Mol Spectrosc, http://dx.doi.org/10.1016/j.jms.2013.06.003 [in press].

[8] Niederer HM, Albert S, Bauerecker S, Boudon V, Champion J-P, Quack M. Global analysis of the infrared spectrum of $^{13}CH_4$: lines in the region 0 to 3200 cm^{-1}. Chimia 2008;62:273–6.

[9] Rothman LS, Gordon IE, Babikov Y, Barbe A, Benner DC, Bernath PF, et al. The HITRAN 2012 molecular spectroscopic database. J Quant Spectrosc Radiat Transfer, http://dx.doi.org/10.1016/j.jqsrt.2013.07.002 [in this issue].

[10] Rothman LS, Gordon IE, Barbe A, Benner DC, Bernath PF, Birk M, et al. The HITRAN 2008 molecular spectroscopic database. J Quant Spectrosc Radiat Transfer 2009;110:533–72.

[11] Rothman LS, Jacquemart D, Barbe A, Benner DC, Birk M, Brown LR, et al. The HITRAN 2004 molecular spectroscopic database. J Quant Spectrosc Radiat Transfer 2005;92:139–207.

[12] Rothman LS, Barbe A, Benner DC, Brown LR, Camy-Peyret C, Carleer MR, et al. The HITRAN molecular spectroscopic database: edition of 2000 including updates through 2001. J Quant Spectrosc Radiat Transfer 2003;82:5–44.

[13] Rothman LS, Rinsland CP, Goldman A, Massie ST, Edwards DP, Flaud J-M, et al. The 1996 HITRAN molecular spectroscopic database and HAWKS (HITRAN Atmospheric workstation). J Quant Spectrosc Radiat Transfer 1998;60:665–710.

[14] Rothman LS, Gamache RR, Tipping RH, Rinsland CP, Smith MAH, Benner DC, et al. The HITRAN molecular database: editions of 1991 and 1992. J Quant Spectrosc Radiat Transfer 1992;48:469–507.

[15] Rothman LS, Smith MAH, Goldman A, Brown LR, Toth RA, Pickett HM, et al. The HITRAN database: 1986 edition. Appl Opt 1987;26:4058–97.

[16] Rothman LS, Gamache RR, Barbe A, Goldman A, Gillis JR, Brown LR, et al. AFGL atmospheric absorption line parameters compilation: 1982 edition. Appl Opt 1983;22:2247–56.

[17] McClatchey RA, Benedict WS, Clough SA, Burch DE, Fox K, Rothman LS, et al. AFCRL atmospheric absorption line parameters compilation. AFCRL-TR-73-0096. Environmental Research Papers no. 434; 1973.

[18] Boudon V, Pirali O, Roy P, Brubach J-B, Manceron L, Vander Auwera J. The high-resolution far-infrared spectrum of methane at the SOLEIL synchrotron. J Quant Spectrosc Radiat Transfer 2010;111:1117–29.

[19] Abe M, Iwakuni K, Okubo S, Sasada H. Accurate transition frequency list of the ν_3 band of methane from sub-Doppler resolution comb-referenced spectroscopy. J Opt Soc Am B 2013;30:1027–35 [and the references therein].

[20] Nikitin AV, Daumont L, Thomas X, Régalia L, Rey M, Tyuterev VlG, et al. Preliminary assignments of $2\nu_3-\nu_4$ hot band of the $^{12}CH_4$ in the 2 μm transparency window from long-path FTS spectra. J Mol Spectrosc 2011;268:93–106.

[21] Nikitin AV, Brown LR, Rey M, Tyuterev VlG, Sung K, Smith MAH, et al. Preliminary modeling of CH_3D from 4000 to 4550 cm^{-1}. J Quant Spectrosc Radiat Transfer 2013;114:1–12.

[22] Wishnow EH, Orton GS, Ozier I, Gush HP. The distortion dipole rotational spectrum of CH_4: a low temperature far-infrared study. J Quant Spectrosc Radiat Transfer 2007;103:102–17.

[23] Cassam-Chenai P, Liévin J. *Ab initio* calculation for the rotational spectrum of methane vibrational ground state. J Chem Phys 2012;136:174309-1–15.

[24] Okubo S, Nakayama H, Iwakuni K, Inaba H, Sasada H. Absolute frequency list of the ν_3-band transitions of methane at a relative uncertainty level of 10^{-11}. Opt Exp 2011;19:23878–88.

[25] Tsuji K, Teshima H, Sasada H, Yoshida N. Spectroscopic isotope ratio measurement of doubly-substituted methane. Spectrochim Acta Pt A 2012;98:43–6 [and references therein].

[26] Ishibashi C, Kourogi M, Imai K, Bambang W, Onae A, Sasada H. Absolute frequency measurement of the saturated absorption lines of methane in the 1.66 μm region. Opt Commun 1999;161:223–6.

[27] Predoi-Cross A, Brawley-Tremblay M, Brown LR, Devi VM, Benner DC. Multispectrum analysis of $^{12}CH_4$ from 4100 to 4635 cm^{-1}: II. Air-broadening coefficients (widths and shifts). J Mol Spectrosc 2006;236:201–15.

[28] Ulenikov ON, Bekhtereva ES, Albert S, Bauerecker S, Hollenstein H, Quack M. High resolution infrared spectroscopy and global vibrational analysis for the CH_3D and CHD_3 isotopomers of methane. Mol Phys 2010;108:1209–40.

[29] Nikitin AV, Champion J-P, Tyuterev VlG. The MIRS computer package for modeling the ro-vibrational spectra of polyatomic molecules. J Quant Spectrosc Radiat Transfer 2003;82:239–49.

[30] Brown LR. Empirical line parameters of methane from 1.1 to 2.1 μm. J Quant Spectrosc Radiat Transfer 2005;96:251–70.

[31] Nikitin A, Lyulin O, Mikhailenko S, Perevalov V, Filippov N, Grigoriev I, et al. GOSAT-2009 methane spectral list in the 5550–6236 cm^{-1} range. J Quant Spectrosc Radiat Transfer 2010;111:2211–24.

[32] Campargue A, Leshchishina O, Wang L, Mondelain D, Kassi S. The WKLMC empirical line lists (5852–7919 cm^{-1}) for methane between 80 K and 296 K: "final" lists for atmospheric and planetary applications. J Mol Spectrosc 2013;. http://dx.doi.org/10.1016/j.jms.2013.03.001 [in press].

[33] Campargue A, Leshchishina O, Wang L, Mondelain D, Kassi S, Coustenis A. An improved empirical line list for methane in the region of the $2\nu_3$ band at 1.66 μm. J Quant Spectrosc Radiat Transfer 2013;118:49–59.

[34] Margolis JS. Measured line positions and strengths of methane from 5500 to 6180 cm^{-1}. Appl Opt 1988;27:4038–51.

[35] Margolis JS. Empirical values of the ground-state energies for methane transitions between 5500 and 6150 cm^{-1}. Appl Opt 1990;29:2295–302.

[36] Campargue A, Leshchishina O, Wang L, Mondelain D, Kassi S, Nikitin AV. Refinements of the WKMC empirical line lists (5852–7919 cm^{-1}) for methane between 80 K and 296 K. J Quant Spectrosc Radiat Transfer 2012;113:1855–73.

[37] Campargue A, Leshchishina O, Mondelain D, Kassi S, Coustenis A. An improved empirical line list for methane in the region of the $2\nu_3$ band at 1.66 μm. J Quant Spectrosc Radiat Transfer 2013;118:49–59.

[38] Campargue A, Wang L, Kassi S, Mondelain D, Bézard B, Lellouch E, et al. An empirical line list for methane in the 1.26–1.71 μm region for planetary investigations (T=80–300 K). Application to Titan. Icarus 2012;219:110–28.

[39] Gao B, Kassi S, Campargue A. Empirical low energy values for methane transitions in the 5852-6181 cm^{-1} region by absorption spectroscopy at 81 K. J Mol Spectrosc 2009;253:55–63.
[40] Wang L, Kassi S, Campargue A. Temperature dependence of the absorption spectrum of CH_4 in the region of the $2\nu_3$ band at 1.66 μm by absorption spectroscopy at 81 K. J Quant Spectrosc Radiat Transfer 2010;111:1130–40.
[41] Sciamma-O'Brien E, Kassi S, Gao B, Campargue A. Experimental low energy values of CH_4 transitions near 1.33 μm by absorption spectroscopy at 81 K. J Quant Spectrosc Radiat Transfer 2009;110: 951–63.
[42] Campargue A, Wang L, Kassi S, Mašát M, Votava O. Temperature dependence of the absorption spectrum of CH_4 by high resolution spectroscopy at 81 K: (II) the Icosad region (1.49–1.30 μm). J Quant Spectrosc Radiat Transfer 2010;111:1141–51.
[43] Votava O, Mašát M, Pracna P, Kassi S, Campargue A. Accurate determination of low state rotational quantum numbers ($J<4$) from planar-jet and liquid nitrogen cell absorption spectra of methane near 1.4 μm. Phys Chem Chem Phys 2010;12:3145–55.
[44] Wang L, Mondelain D, Kassi S, Campargue A. The absorption spectrum of methane at 80 and 294 K in the Icosad (6717–7589 cm^{-1}): improved empirical line lists, isotopologue identification and temperature dependence. J Quant Spectrosc Radiat Transfer 2011;113:47–57.
[45] Liu AW, Kassi S, Campargue A. High sensitivity CW-cavity ring down spectroscopy of CH_4 in the 1.55 μm transparency window. Chem Phys Lett 2007;447:16–20.
[46] Wang L, Kassi S, Liu AW, Hu SM, Campargue A. High sensitivity absorption spectroscopy of methane at 80 K in the 1.58 μm transparency window: temperature dependence and importance of the CH_3D contribution. J Mol Spectrosc 2010;261:41–52.
[47] Campargue A, Wang L, Liu AW, Hu SM, Kassi S. Empirical line parameters of methane in the 1.63–1.48 μm transparency window by high sensitivity Cavity Ring Down Spectroscopy. Chem Phys 2010;373:203–10.
[48] Nikitin AV, Thomas X, Régalia L, Daumont L, Von der Heyden P, Tyuterev VIG, et al. First assignment of the $5\nu_4$ and $\nu_2+4\nu_4$ band systems of $^{12}CH_4$ in the 6287–6550 cm^{-1} region. J Quant Spectrosc Radiat Transfer 2011;112:28–40.
[49] Wang L, Kassi S, Liu AW, Hu SM, Campargue A. The 1.58 μm transparency window of methane (6165-6750 cm^{-1}): empirical line list and temperature dependence between 80 K and 296 K. J Quant Spectrosc Radiat Transfer 2011;112:937–51.
[50] Mondelain D, Kassi S, Wang L, Campargue A. The 1.28 μm transparency window of methane (6165–6750 cm^{-1}): empirical line list and temperature dependence between 80 K and 296 K. Phys Chem Chem Phys 2011;17:7985–96.
[51] Kassi S, Gao B, Romanini D, Campargue A. The near infrared (1.30–1.70 μm) absorption spectrum of methane down to 77 K. Phys Chem Chem Phys 2008;10:4410–9.
[52] Lu Y, Mondelain D, Kassi S, Campargue A. The CH_3D absorption spectrum in the 1.58 μm transparency window of methane: empirical line lists and temperature dependence between 80 K and 296 K. J Quant Spectrosc Radiat Transfer 2011;112:2683–97.
[53] Zolot AM, Giorgetta FR, Baumann E, Swann WC, Coddington I, Newbury NR. Broad-band frequency references in the near-infrared: accurate dual comb spectroscopy of methane and acetylene. J Quant Spectrosc Radiat Transfer 2013;118:26–39.
[54] Lyulin OM, Kassi S, Sung K, Brown LR, Campargue A. Determination of the low energy values of $^{13}CH_4$ transitions in the $2\nu_3$ region near 1.66 μm from absorption spectra at 296 and 81 K. J Mol Spectrosc 2010;261:91–100.
[55] Lutz BL, de Bergh C, Maillard JP. Monodeuterated methane in the outer solar system. I. Spectroscopic analysis of the bands at 1.55 and 1.95 μm. Astrophys J 1983;273:397–409.
[56] Boussin C, Lutz BL, de Bergh C, Hamdouni A. Line intensities and self-broadening coefficients for the $3\nu_2$ band of monodeutrated methane. J Quant Spectrosc Radiat Transfer 1998;60:501–14.
[57] Boussin C, Lutz BL, Hamdouni A, de Bergh C. Pressure broadening and shift coefficients for H_2, He and N_2 in the $3\nu_2$ band of $^{12}CH_3D$ retrieved by a multispectrum fitting technique. J Quant Spectrosc Radiat Transfer 1999;63:49–84.
[58] Manca Tanner C, Quack M. Reinvestigation of $\nu_2+2\nu_3$ subband in the overtone icosad of $^{12}CH_4$ using cavity ring-down (CRD) spectroscopy of a supersonic jet expansion. Mol Phys 2012;110:2111–35.
[59] Hippler M, Quack M. High-resolution Fourier transform infrared and cw-diode laser cavity ringdown spectroscopy of the $\nu_2+2\nu_3$ band of methane near 7510 cm^{-1} in slit jet expansions and at room temperature. J Chem Phys 2002;116:6045–55.
[60] de Bergh C, Courtin R, Bézard B, Coustenis C, Lellouch E, Hirtzig M, et al. Applications of a new set of methane line parameters to the modeling of Titan's spectrum in the 1.58-micron window. Planet Space Sci 2012;61:85–99.
[61] Bailey J, Ahlsved L, Meadows VS. The near-IR spectrum of Titan modelled with an improved methane line list. Icarus 2011;213:218–32.
[62] Lellouch E, Sicardy B, de Bergh C, Käufl H-U, Kassi S, Campargue A. Pluto's lower atmosphere structure and methane abundance from high-resolution spectroscopy and stellar occultations. Astron Astrophys 2009;495:17–21.
[63] Irwin PGJ, de Bergh C, Courtin R, Bézard B, Teanby NA, Davis GR, et al. The application of new methane line absorption data to Gemini-N/NIFS and KPNO/FTS observations of Uranus' near-infrared spectrum. Icarus 2012;220:369–82.
[64] Sromovsky LA, Fry PM, Boudon V, Campargue A, Nikitin AV. Comparison of line-by-line and band models of near-IR methane absorption applied to outer planet atmospheres. Icarus 2012;218:1–23.
[65] Benner DC, Devi VM, O'Brien JJ, Shaji S, Spickler PT, Houck CP, et al. Empirical line parameters of CH_4 from 10923 to 11502 cm^{-1} [in preparation].
[66] O'Brien JJ, Hong C. Absorption spectra and absorption coefficients for methane in the 750–940 nm region obtained by intracavity laser spectroscopy. J Quant Spectrosc Radiat Transfer 2002;75:323–50.
[67] Benner DC, Rinsland CP, Devi VM, Smith MAH, Atkins D. A multispectrum nonlinear least squares fitting technique. J Quant Spectrosc Radiat Transfer 1995;53:705–21.
[68] Antony BK, Niles DL, Wroblewski SB, Humphrey CM, Gabard T, Gamache RR. N_2-, O_2- and air-broadened half-widths and line shifts for transitions in the ν_3 band of methane in the 2276- to 3200-cm^{-1} spectral region. J Mol Spectrosc 2008;251:268–81.
[69] Sanzharov M, Vander Auwera J, Pirali O, Roy P, Brubach J-B, Manceron L, et al. Self and N_2 collisional broadening of far-infrared methane lines measured at the SOLEIL synchrotron. J Quant Spectrosc Radiat Transfer 2012;113:1874–86.
[70] Smith MAH, Benner DC, Predoi-Cross A, Devi VM. Multispectrum analysis of $^{12}CH_4$ in the ν_4 spectral region: I. Air-broadened half widths, pressure-induced shifts, temperature dependences and line mixing. J Quant Spectrosc Radiat Transfer 2009;110:639–53.
[71] Smith MAH, Benner DC, Predoi-Cross A, Devi VM. Multispectrum analysis of $^{12}CH_4$ in the ν_4 spectral region: II. Self-broadened half widths, pressure-induced shifts, temperature dependences and line mixing. J Quant Spectrosc Radiat Transfer 2010;111:1152–66.
[72] Smith MAH, Benner DC, Predoi-Cross A, Devi VM. A multispectrum analysis of the ν_4 band of $^{13}CH_4$: widths, shifts, and line mixing coefficients. J Quant Spectrosc Radiat Transfer 2011;112:952–68.
[73] Smith MAH, Benner DC, Predoi-Cross A, Devi VM. Air and self-broadened half-widths, pressure-induced shifts and line mixing in the ν_2 band of $^{12}CH_4$. J Quant Spectrosc Radiat Transfer 2013 [accepted for publication].
[74] Predoi-Cross A, Unni AV, Heung H, Devi VM, Benner DC, Brown LR. Line mixing effects in the $\nu_2+\nu_3$ band of methane. J Mol Spectrosc 2007;246:65–76.
[75] Lyulin OM, Perevalov VI, Morino I, Yokota T, Kumazawa R, Watanabe T. Measurements of self-broadening and self-pressure-induced shift parameters of the methane spectral lines in the 5556–6166 cm^{-1} range. J Quant Spectrosc Radiat Transfer 2011;112:531–9.
[76] Lyulin OM, Nikitin AV, Perevalov VI, Morino I, Yokota T, Kumazawa R, et al. Measurements of the N_2- and O_2-broadening and shifting parameters of methane spectral lines in the 5550–6236 cm^{-1} region. J Quant Spectrosc Radiat Transfer 2009;110:654–68.
[77] Gabard T, Boudon V. Line broadening coefficient calculations for methane perturbed by nitrogen. J Quant Spectrosc Radiat Transfer 2010;111:1328–43.
[78] Gabard T. Calculated line broadening parameters for methane perturbed by diatomic molecules. J Mol Spectrosc 2013;. http://dx.doi.org/10.1016/j.jms.2013.05.011 [in press].
[79] Boussin C, Lutz BL, Hamdouni A, de Bergh C. Pressure broadening and shift coefficients for H_2, He and N_2 in the $3\nu_2$ band of $^{12}CH_3D$ retrieved by a multispectrum fitting technique. J Quant Spectrosc Radiat Transfer 1999;63:49–84.
[80] Devi VM, Benner DC, Smith MAH, Rinsland CP, Brown LR. Measurements of air broadening, pressure shifting and off diagonal relaxation matrix coefficients in the ν_3 band of $^{12}CH_3D$. J Mol Struct 2000;517:455–75.
[81] Devi VM, Benner DC, Smith MAH, Rinsland CP. Measurements of air broadened width and air induced shift coefficients and line mixing in the ν_6 band of $^{12}CH_3D$. J Quant Spectrosc Radiat Transfer 2001;68:1–14.

[82] Devi VM, Benner DC, Smith MAH, Rinsland CP. Measurements of air broadened width and air induced shift coefficients and line mixing in the ν_5 band of $^{12}CH_3D$. J Quant Spectrosc Radiat Transfer 2001;68:135–61.
[83] Devi VM, Benner DC, Smith MAH, Rinsland CP, Brown LR. Multispectrum analysis of self- and N_2-broadening, pressure-shifting, and line-mixing in the ν_3 parallel band of $^{12}CH_3D$. J Quant Spectrosc Radiat Transfer 2002;73:603–40.
[84] Devi VM, Benner DC, Brown LR, Smith MAH, Rinsland CP, Sams RL, et al. Multispectrum analysis of self- and N_2-broadening, shifting and line mixing coefficients in the ν_6 band of $^{12}CH_3D$. J Quant Spectrosc Radiat Transfer 2002;72:139–91.
[85] Devi VM, Benner DC, Smith MAH, Rinsland CP, Brown LR. Self- and nitrogen-broadening, pressure induced shift and line mixing coefficients in the ν_5 of $^{12}CH_3D$ using a multi-spectrum fitting procedure. J Quant Spectrosc Radiat Transfer 2002;74:1–41.
[86] Predoi-Cross A, Hambrook K, Brawley-Tremblay S, Bouanich J-P, Devi VM, Benner DC, et al. Measurements and theoretical calculations of self-broadening and self-shift coefficients in the ν_2 band of CH_3D. J Mol Spectrosc 2005;234:53–74.
[87] Predoi-Cross A, Hambrook K, Brawley-Tremblay S, Bouanich J-P, Smith MAH. Measurements and theoretical calculations of N_2-broadening and N_2-shift coefficients in the ν_2 band of CH_3D. J Mol Spectrosc 2006;235:35–53.
[88] Predoi-Cross A, Hambrook K, Brawley-Tremblay S, Bouanich J-P, Devi VM, Smith MAH. Room-temperature broadening and pressure-shift coefficients in the ν_2 band of CH_3D–O_2: measurements and semi-classical calculations. J Mol Spectrosc 2006;236:75–90.
[89] Predoi-Cross A, Brawley-Tremblay S, Povey C, Smith MAH. Experimental air-broadened line parameters in the ν_2 band of CH_3D. Can J Phys 2007;85:199–218.
[90] Brown LR, Margolis JS, Champion JP, Hilico JC, Jouvard JM, Loëte M, et al. Methane and its isotopes: current status and prospects for improvement. J Quant Spectrosc Radiat Transfer 1992;48:617–28.
[91] Brown LR, Benner DC, Champion JP, Devi VM, Fejard L, Gamache RR, et al. Methane line parameters in HITRAN. J Quant Spectrosc Radiat Transfer 2003;82:219–38.
[92] Frankenberg C, Warneke T, Butz A, Aben I, Hase F, Spietz P, et al. Methane spectroscopy in the near infrared and it simplification on atmospheric retrievals. Atmos Chem Phys 2008;8:5061–75.
[93] Tran H, Hartmann J-M, Toon G, Brown LR, Frankenberg C, Warneke T, et al. The $2\nu_3$ band of CH_4 revisited with line mixing. Consequences for spectroscopy and atmospheric retrievals at 1.67 μm. J Quant Spectrosc Radiat Transfer 2010;111:1344–56.
[94] Kapitanov VA, Osipov A, Yu K, Protasevich AE, Ponomarev YuN. Collisional parameters of N_2 broadened methane lines in the R9 multiplet of the $2\nu_3$ band. Multispectrum fittings of the overlapping spectral lines. J Quant Spectrosc Radiat Transfer 2012;113:1985–92.
[95] Osipov A, Protasevich AE, Kapitanov VA, Ponomarev VA, Ponurovskii YY. Collision parameters of N_2-broadened methane lines in R_5 multiplet of $2\nu_3$ band. Multispectrum fitting of overlapping spectral lines. Appl Phys B: Lasers Opt 2012;105:725–32 [and references therein].
[96] Marquardt R, Quack M. Global analytical potential hypersurface for large amplitude nuclear motion and reactions in methane II. Characteristic properties of the potential and comparison to other potentials and experimental information. J Phys Chem A 2004;108:3166–81.
[97] Marquardt R, Quack M. Global analytical potential energy surfaces for high resolution molecular spectroscopy and reaction dynamics. In: Quack M, Merkt F, editors. Handbook of high-resolution spectroscopy, vol. 1. Chichester, New York. ISBN: 978-0-470-06653-9. p. 511–49 [Chapter 12].
[98] Schwenke DW, Partridge H. Vibrational energy levels for CH_4 from an *ab initio* potential. Spectrochim Acta A 2001;57:887–95.
[99] Schwenke DW. Towards accurate *ab initio* predictions of the vibrational spectrum of methane. Spectrochim Acta A 2002;58:849–61.
[100] Wang XG, Carrington T. Computing rovibrational levels of methane with curvilinear internal vibrational coordinates and an Eckart frame. J Chem Phys 2013;138:104106.
[101] Yurchenko S, Tennyson J, Barber RJ, Thiel W. Variational transition moments of CH_4 from first principles. J Mol Spectrosc 2013;. http://dx.doi.org/10.1016/j.jms.2013.05.014 [in press].
[102] Nikitin AV, Rey M, Tyuterev VlG. Rotational and vibrational energy levels of methane calculated from a new potential energy surface. Chem Phys Lett 2011;501:179–86.
[103] Nikitin AV, Rey M, Tyuterev VlG. New dipole moment surfaces of methane. Chem Phys Lett 2013;565:5–11.
[104] Rey M, Nikitin AV, Tyuterev VlG. Predictions for methane spectra from potential energy and dipole moment surfaces: isotopic shifts and comparative study of $^{13}CH_4$ and $^{12}CH_4$. J Mol Spectrosc 2013;. http://dx.doi.org/10.1016/j.jms.2013.04.003 [in press].
[105] Cassam-Chenai P, Bouret P, Rey M, Tashkun SA, Nikitin AV, Tyuterev VlG. *Ab initio* effective rotational hamiltonians: a comparative study. Int J Quant Chem 2012;112:2201–20.
[106] Tyuterev VlG, Tashkun, S, Nikitin AV, Rey M, Kochanov R. Spectroscopic models for methane polyads derived from a potential energy surface: extension to higher quantum numbers. In: Workshop on "Spectroscopy of methane for atmospheric and planetary applications"; 2012. ⟨http://www.icb.cnrs.fr/titan/documents/Workshop_ter/Tyuterev.pdf⟩.
[107] Rey M, Nikitin AV, Tyuterev VlG. Complete nuclear motion Hamiltonian in the irreducible normal mode tensor operator formalism for the methane molecule. J Chem Phys 2012;136:244106.
[108] Rey M, Nikitin AV, Tyuterev VlG. First-principles intensity calculations for the methane rovibrational spectra in the infrared. Phys Chem Chem Phys 2013;15:10049–61.
[109] Borysov A, Champion J-P, Jørgensen UG, Wenger C. Towards simulation of high temperature methane spectra. Mol Phys 2002;100:3585–94.
[110] Nikitin AV, Rey M, Champion JP, Tyuterev VlG. Extension of the MIRS computer package for the modeling of molecular spectra: from effective to full *ab initio* ro-vibrational Hamiltonians in irreducible tensor form. J Quant Spectrosc Radiat Transfer 2012;113:1034–42.
[111] Boudon V, Champion JP, Gabard T, Loete M, Rotger M, Wenger C. Spherical top theory and molecular spectra, Handbook of High Resolution Spectroscopy, Quack M, Merkt F, editors. vol 3, pp. 1437-60, Wiley, Chichester, New York. 2011.
[112] Brogi M, Snellen IAG, de Kok RJ, Albrecht S, Birkby JL, de Mooij EJW. Detection of molecular absorption in the dayside of exoplanet 51 PEGASI. Astrophys J 2013;767:27–37.
[113] Hartman J-M, Boulet C, Robert D. Collisional effects on molecular spectra: laboratory experiments and models, consequences for applications. Amsterdam: Elsevier; 2008.
[114] Mondelain D, Payan S, Deng W, Camy-Peyret C, Hurtmans D, Mantz AW. Measurement of the temperature dependence of line mixing and pressure broadening parameters between 296 and 90 K in the ν_3 band of $^{12}CH_4$ and their influence on atmospheric methane retrievals. J Mol Spectrosc 2007;244:130–7.
[115] Boone CD, Walker KA, Bernath PF. An efficient analytical approach for calculating line mixing in atmospheric remote sensing applications. J Quant Spectrosc Radiat Transfer 2011;112:980–9.
[116] Pine AS. N_2 and Ar broadening and line mixing in the P and R branches of the ν_3 band of CH_4. J Quant Spectrosc Radiat Transfer 1997;57:157–76.
[117] Pine AS, Gabard T. Speed-dependent broadening and line mixing in CH_4 perturbed by Ar and N_2 from multispectrum fits. J Quant Spectrosc Radiat Transfer 2000;66:69–92.
[118] Pine AS, Gabard T. Multispectrum fits for line mixing in the ν_3 band Q branch of methane. J Mol Spectrosc 2003;217:105–14.
[119] Tran H, Flaud P-M, Gabard T, Hase F, von Clarmann T, Camy-Peyret C, et al. Model, software and database for line-mixing effects in the ν_3 and ν_4 bands of CH_4 and tests using laboratory and planetary measurements–I: N_2 (and air) broadenings and the earth atmosphere. J Quant Spectrosc Radiat Transfer 2006;101:284–305.
[120] Tran H, Flaud P-M, Fouchet T, Gabard T, Hartmann J-M. Model, software and database for line-mixing effects in the ν_3 and ν_4 bands of CH_4 and tests using laboratory and planetary measurements–II: H_2 (and He) broadenings and the atmospheres of Jupiter and Saturn. J Quant Spectrosc Radiat Transfer 2006;101:306–24.
[121] Hill C, Gordon IE, Rothman LS, Tennyson J. A new relational database structure and online interface for the HITRAN database. J Quant Spectrosc Radiat Transfer, http://dx.doi.org/10.1016/j.jqsrt.2013.04.027 [in this issue].
[122] Dubernet ML, Boudon V, Culhane JL, Dimitrijevic MS, Fazliev AZ, Joblin C, et al. Virtual Atomic and Molecular Data Centre. J Quant Spectrosc Radiat Transfer 2010;111(2010):2151–9.